ORIGINAL ARTICLE

lajss.org Latin American Journal of Solids and Structures

www.lajss.org

# Adaptive enhanced proportional topology optimization algorithm and its engineering application

**Jiao Wang[a]***

[a] School of Mathematics and Statistics, Weinan Normal University, Shaanxi, Weinan, 714099, China. Email: wjiao91@163.com

* Corresponding author

https://doi.org/10.1590/1679-7825/e9196

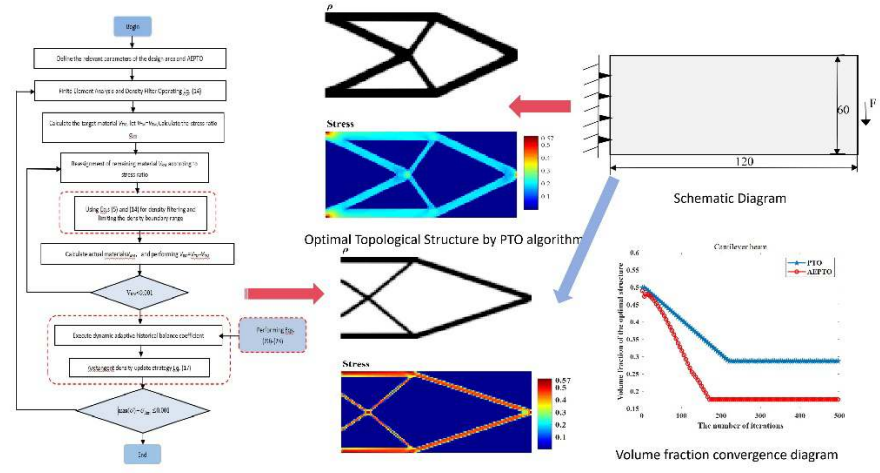
## Abstract

This paper proposes an adaptive enhanced proportional topology optimization algorithm (AEPTO) to address the problems of poor convergence, multiple grayscale units, and unclear topology structure in handling stress constrained minimum volume problems using the proportional topology optimization algorithm (PTO). This algorithm systematically improves the PTO algorithm in terms of interpolation method, filtering processing, density update, and convergence control by introducing a new material interpolation model based on logistic function, Cauchy type density filter, arctangent density update strategy, and dynamic adaptive historical balance coefficient. Through numerical experiments on topology optimization of three typical structures, namely cantilever beams, L-shaped beams, and MBB beams, under stress constraints, it is shown that the AEPTO algorithm significantly reduces the volume fraction of the structure, improves convergence speed, reduces the number of gray units, and the optimized topology structure is clearer and the material distribution is more reasonable. It has good engineering applicability and optimization efficiency, providing an effective gradient free optimization method for lightweight structural design.

## Keywords

Proportional topology optimization algorithm, Cauchy type density filter, Arctangent density update strategy, Dynamic adaptive historical balance coefficient, Topology structure.

## Graphical abstract




Received July 04, 2026. In revised form July 08, 2026. Accepted July 27, 2026. Available online July 30, 2026.
https://doi.org/10.1590/1679-7825/e9196

Latin American Journal of Solids and Structures. ISSN 1679-7825. Copyright © 2026. This is an Open Access article distributed under the terms of the Creative Commons Attribution License, which permits unrestricted use, distribution, and reproduction in any medium, provided the original work is properly cited.

## 1 INTRODUCTION

Lightweight design is not only the inevitable requirement of the development of modern engineering technology, but also the pursuit of the field of structural design by Holmberg et al. (2013). In order to realize lightweight design, structural optimization methods, namely shape optimization, size optimization and topology optimization, are proposed. The effectiveness of these methods is also verified by solving various optimization problems. Topology optimization is different from the other two methods, which can provide the best conceptual design of structural material layout in the early stage of structural design, so that structural design can minimize the weight of the structure by Jang et al. (2014) and Li et al. (2015). Although the designs obtained by topology optimization methods generally require post-processing to meet practical application needs, their prominent advantage lies in the elimination of the need for an initial design. Based on these advantages, topology optimization is favored by academia and widely used in aerospace, biomedicine, civil engineering, additive manufacturing and other fields. Topology optimization is a basic theory of structure, which is established by combining computer technology, topology and basic theory of optimization methods. It involves computational mechanics, mathematics, image processing and visualization, numerical method research and other fields and technologies. Owing to its widespread application in fields such as structural engineering, automotive engineering, mechanical engineering, aerospace manufacturing, and materials science, topology optimization has emerged as one of the fastest-growing research areas. Topology optimization refers to finding the best force transmission path of the structure or the optimal distribution of materials in the given area under the given load, boundary, stress, displacement and other constraints, reducing the weight of the structure to save costs, and improving the performance of the structure. The essence of topology optimization can be understood as the process of removing invalid or inefficient materials while retaining effective materials. Its most salient feature is the ability to obtain the lightest-weight structural configuration when the structural topology is unknown, without relying on any human experience or a priori knowledge.

In the past decades, topology optimization has made various important progress. Research progress on topology optimization methods can refer to literature by Sigmund and Maute (2013) and Van Dijk et al. (2013). Most of the research on topology optimization focuses on solving the minimum flexibility optimization problem, making the structure achieve the best stiffness, and even extending to the problems related to volume, displacement and frequency. However, although stress plays a very important role in ensuring the safety of the structure in the process of use, people pay relatively little attention to the optimization problem of stress constraints. This may be due to some challenging problems (such as high nonlinearity and local properties of stress constraints) are difficult to overcome when solving stress constrained optimization problems (París et al. 2009; Luo et al. 2013; Lee et al. 2016).

Topology optimization can be divided into discrete topology optimization and continuum topology optimization for the research object. The discrete body generally refers to the optimization of the member system. It pays attention to the number of elements and the connection mode of nodes in the structure. The topology of the discrete body is relatively mature. A continuum refers to a planar or three-dimensional solid structure, whose focus lies in the external boundaries of the structural material, the presence or absence of voids within the material, and the distribution of such voids. Continuum topology optimization is a process that divides the entire solid object under study into individual elements, then determines the existence of each element under given constraints using a specific optimization algorithm, removes invalid elements, and retains valid ones, thereby forming a series of voids in the solid structure. In recent years, continuum topology has developed rapidly and become the focus of researchers and scholars. The current research direction mainly includes the following points: description of topological structure and establishment of interpolation model; Numerical solution method of topology optimization and application of new algorithm; The method of removing instability and the extraction and reconstruction of optimized structure; Practical application research.

Despite the rapid development of structural topology optimization, further research is still needed, such as topological solving techniques. At present, many topology optimization technologies have been developed to solve the above two types of problems. Such methods can be broadly classified into two categories based on the requirement for gradient information: gradient-based optimization methods, and gradient-free algorithms including Genetic Algorithms, Ant Colony Optimization, Particle Swarm Optimization, Neural Network Algorithms, and the Proportional Topology Optimization (PTO) algorithm.

According to the research results of numerical optimization methods, it can be seen that the optimization method based on sensitivity is very popular in solving various optimization problems. For instance, Optimality Criteria (OC) method (Vemaganti and Lawrence 2005), Sequential Linear Programming (SLP) method (Dantzig 1963), Convex Linearization (CONLIN) method (Fleury and Braibant 1986), and the Method of Moving Asymptotes (MMA) (Svanberg 1987) all require the calculation of gradient information for the objective function and constraint conditions. Gradient information is easy to obtain for general continuous differentiable functions. However, it is difficult to obtain accurate gradient information if the derivation of stress problems or more complex topology optimization problems is very complex.

In addition, the calculation of gradient information may bring additional computational burden, which may lead to some problems that are not conducive to the implementation of optimization algorithm (Biyikli and To 2015). Therefore, non-sensitive optimization methods such as genetic algorithm (Madeira et al. 2005), annealing algorithm (Garcia-Lopez et al. 2011), ant colony algorithm (Yoo and Han 2015) and proportional topology optimization (PTO) algorithm (Biyikli and To 2015) are increasingly favored by many scholars. For continuum topology optimization problems, the PTO method offers a more intuitive and straightforward solution. This method does not need the sensitivity information of the correlation function in the design model, avoids the complexity related to the sensitivity information, and not only effectively suppresses the gray area, but also improves the target. In addition, it can directly solve the 0/1 problem without penalty, post-processing or filtering. On the contrary, the most obvious disadvantage is the large number of design combinations, which hinders the effectiveness of the search process. In short, there is a trade-off between sensitivity and non-sensitivity methods in terms of complexity and efficiency of calculation/implementation by Lee and Geem (2004).

Combining the characteristics of SIMP and bionic intelligent algorithm, Biyikli proposed a simple and effective non-sensitive PTO to solve the stress constraint and minimum compliance topology optimization problems. The PTO algorithm assigns design variables to elements in proportion to the stress value in the stress problem and the compliance in the compliance problem. In particular, impose global constraints on the whole system. The PTO method is highly heuristic and can find optimized solutions.It is this heuristic method that renders the algorithm easy to interpret and implement, allowing us to obtain effective and accurate solutions. It is worth noting that although PTO is highly heuristic, its performance is much better than that of random method, which will be proved by comparing its efficiency with mathematical method. Based on the above analysis, PTO can also be called an intelligent optimization algorithm with targeted objects, which is specially used to solve structural topology problems. Although PTO has the same characteristics as bionic intelligent algorithms, such as no need of sensitivity information, high efficiency and accuracy, and simple, but it also has disadvantages such as poor robustness, relatively poor topology, and relatively poor ability of penalty density variable of 0 or 1 (Li et al. 2024; Amaral et al. 2022; Hussain et al. 2025; Nguyen et al. 2023).

In order to overcome the shortcomings of PTO algorithm, aiming at the minimum volume fraction problem, this paper modifies the interpolation model, filter and density variable update scheme, the update method of density variable in the inner loop and main loop, and adds the dynamic adaptive balance coefficient. Three numerical examples show the effectiveness and practicability of the improved scheme. The remaining research contents are as follows: in Section 2, the mathematical model of topology optimization is given. Section 3 outlines the proportional topology optimization algorithm. Section 4 presents the adaptive enhanced proportional topology optimization algorithm (AEPTO), and the specific flowchart is given. Three classical beam problems are solved by AEPTO in the Section 5. Section 6 summarizes the full text.

## 2 MATHEMATICAL MODEL OF TOPOLOGY OPTIMIZATION

With the better resolution of compliance optimization problems in topology optimization, an increasing amount of research resources has been gradually devoted to the study of stress-constrained optimization problems. After years of unremitting efforts of scholars in the field of structural optimization design, the research on stress constrained optimization has made certain progress. From the literature proposed by Yang et al. (2018) and Kongwat and Hasegawa (2019), it can be found that in most topology optimization studies involving stress constraints, structural failure is usually avoided by limiting the maximum stress limit. A common goal is to obtain the black-and-white (0/1) optimal structure with the most reasonable material distribution, and minimizing or maximizing the objective function without redundancy by satisfying the constraint conditions.

The purpose of structural topology optimization is to find the optimal distribution of materials that meet the constraint conditions and optimize the objective function of the mathematical model. Before solving the optimization problem, the main task is to build its mathematical model. However, if the designer cannot build the mathematical model accurately according to the requirements of the problem, the optimized results will be greatly affected. The most typical and common problem in topology optimization is compliance, which is to minimize compliance while meeting multiple constraints such as volume fraction. Its specific mathematical model by Guo (2025) is as follows:

$$\text{Min} \quad V(\rho)=\sum_{i=1}^{N}\rho_i v_i \text{ ,} \tag{1}$$

$$\begin{cases} \mathbf{KU} = \mathbf{F}, \\ \sigma_i \le \sigma_{\text{limt}}, if \quad \rho > 0, \\ 0 \le \rho_{\min} \le \rho_i \le \rho_{\max} \le 1. \end{cases} \tag{2}$$

Where $V$ is the objective function about the density variable $\rho$, $v_i$ is the volume of the i-th element, $\rho_i$ is the density variable of the discrete element $i$, **U**, **F** and **K** represent the overall displacement vector, external force vector of the structure and the global stiffness matrix. N is the number of elements obtained in the discrete design domain, $\sigma_i$ is the element stress, which is taken as the von Mises stress at the geometric center of the element. The stress is required to not exceed the elastic limit of any element in the system. $\sigma_{\text{limt}}$ (the elastic limit of material) is the maximum limit of element stress, $\rho_{\min}$ and $\rho_{\max}$ represents the upper and lower bounds of $\rho_i$. Usually $\rho_{\max} = 1$ and $\rho_{\min}$ needs to assign a lower limit slightly greater than zero to eliminate the stiffness singularity. The Von Mises support vector path of the element is calculated by the following function:

$$\sigma = \sqrt{\sigma_x^2 + \sigma_y^2 + \sigma_x \sigma_y + 3\sigma_{xy}^2} \ . \tag{3}$$

In practical engineering problems, in order to obtain the ideal topology optimization results, in addition to the material interpolation method, it is also necessary to select the appropriate numerical solution method. A proper numerical solution algorithm can find the optimal solution of topology optimization more quickly and accurately. In order to better solve the stress constraint problem, numerous numerical methods have been proposed by scholars at home and abroad through years of unremitting efforts, among which the gradient-free proportional topology optimization (PTO) method has emerged as one of the most popular approaches at present.

## 3 OVERVIEW OF PROPORTIONAL TOPOLOGY OPTIMIZATION ALGORITHM

The proportional topology optimization (PTO) algorithm was originally proposed by Biyikli and To (2015) as a numerical solution method for topology optimization that globally applies constraints across the entire topology optimization system. PTO algorithm distributes materials to corresponding elements according to the stress ratio of the total stress and the total flexibility of each element. It is a topology optimization algorithm that is easy to understand in theory and easy to realize in program. In addition, PTO algorithm does not include sensitivity calculation, which can effectively avoid the complexity brought by sensitivity in the optimization process. PTO can also be called an intelligent optimization algorithm with targeted objects, which is specially used to solve structural topology problems.

Firstly, the PTO algorithm establishes the vector, matrix of finite element and stress analysis and filtering. Then, the algorithm enters the main loop, and each iteration of the main loop starts with finite element analysis and stress analysis. Finally, the termination criteria will be checked. That is, it is verified whether the maximum elemental stress in the system falls within the allowable stress limit within the specified tolerance range, which is set to 0.001 in this paper. If this condition is satisfied (returns true), the simulation is terminated. Otherwise, the algorithm continues to optimize the topological structure.

### 3.1 Material insertion model

Generally, it is difficult to find a suitable mathematical method to solve the optimization problem of continuum structure based on 0 or 1 discrete variables. If a continuously variable density variable is introduced within the interval [0,1], this problem can be readily solved. At present, many methods have been developed to solve the continuous change of design variables in the interval [0,1]. SIMP method is one of the most popular methods. A penalty factor of power function is introduced to suppress the generation of intermediate density elements, so that the density value of intermediate elements is interpolated to zero or the same as that of interstitial elements or solid elements. It has been widely recognized by the academic community and applied to the field of structural optimization design. SIMP method is also called "material interpolation", "penalty method" or "density" method.

PTO method adopts the modified SIMP approach proposed by Andreassen et al. (2011), which is a density approach that can improve the search performance while maintaining approximate 0/1 solutions. The modified SIMP enhances the relationship between Young's modulus and element density as follows:

$$E(\rho_i) = E_{\min} + \rho_i^{\,p}(E_{\min} - E_0), \rho_i \in [0,1] . \tag{4}$$

Where $E$ is the density-related Young's modulus, and $E_{\min}$ is a very small Young's modulus (usually $10^{-9}$). In order to avoid the occurrence of singular stiffness matrix, $E_0$ is the Young's modulus of solid materials, and *p* is the penalty coefficient (usually 3 ) has a great impact on convergence by Bendsoe and Kikuchi (1988). Compared with standard SIMP method ( $E(\rho_i) = \rho_i^p \cdot E_0$ ), it has no advantages of minimum stiffness and penalty coefficient.

### 3.2 Density filter

Density filtering technology is a common method for normalizing topological optimization problems. Bruns and Tortorelli (2001) introduced this technology into the topological optimization of compliant mechanisms, and proved its effectiveness mathematically. In order to suppress checkerboard patterns, eliminate grid dependency, avoid falling into local minimum and ensure the existence of solutions, density filtering technology is widely used to solve topology optimization problems. The basic idea can be described as follows:

**Step1**: Convert discrete elements in the design domain into density variables that continuously change on the interval [0,1].

**Step2**: Determine the filter radius according to the weight function and calculate the weight coefficient of the target unit.

**Step3**: The filtered density can be obtained by using the density filter function.

For the minimum compliance optimization problem, the PTO algorithm uses a simple cone density filter proposed by Bruns and Tortorelli (2001) as follows:

$$\rho_i = \left(\sum w_{ij} d_j\right) \Big/ \left(\sum w_{ij}\right), \tag{5}$$

$$w_{ij} = \max\{0, 1 - r_{ij} / r_0\} . \tag{6}$$

Where, $\rho_i$ is the filtering density of the *i*-th element, $w_{ij}$ is the filtering weight of elements *i* and *j*, $d_j$ is the non-filtering density of element *j*, $r_{ij}$ is the distance between elements *i* and *j*, $r_0$ is the filter radius, where the sum is the number of cells in the neighborhood, and the weight is inversely proportional to the distance between the element and its adjacent elements. In a sense, cone density filtering is actually only a local average.

### 3.3 Proportional distribution in internal circulation

The update of density variables in the inner ring is also the key to implement stress constraints. The core of the algorithm lies in the calculation and distribution of the Target Material Volume( $V_{\mathrm{TM}}$ ), that is, updating the current material volume to the target material volume. If the maximum element stress is greater than the allowable stress limit, the current amount of material will increase the amount of material movement. Otherwise, it will reduce the same material movement. The material movement volume is related to the number of elements(0.001× the number of elements) and remains constant throughout the simulation process.

$$V_{\mathrm{TM}} = \begin{cases} \sum_{i=1}^{N} \rho_i v_i + 0.001N & \max(\sigma_i) > \sigma_{\mathrm{limt}}, \\ \sum_{i=1}^{N} \rho_i v_i - 0.001N & \max(\sigma_i) \le \sigma_{\mathrm{limt}}. \end{cases} \tag{7}$$

Where *N* is the the number of elements,PTO equates the initial target material quantity $V_{\mathrm{TM}}$ to the remaining material quantity $V_{\mathrm{RM}}$ , then distributes the remaining material quantity in proportion to the element stress value. The calculation equation of unit stress ratio can be see Eq. (8).

$$\sigma_{pro} = \sigma_i^q \Big/ \sum \sigma_i^q v_i . \tag{8}$$

Where, *q* is the proportional index, $\sigma_{pro}$ is the stress ratio matrix. Then the residual volume $V_{\mathrm{RM}}$ is distributed to the corresponding units according to the proportion of the stress of each unit to the total stress of the structure. The distribution equation is the density increment, which can be written as:

$$\Delta\rho_i^{opt} = V_{\mathrm{RM}} \cdot \sigma_{pro} \text{ ,} \tag{9}$$

$\Delta\rho_i^{opt}$ in Eq. (9) is the change amount of the optimized density, the calculation formula of the remaining material volume in Eq. (9) is as follows:

$$V_{\mathrm{RM}} = V_{\mathrm{TM}} - \sum_i \Delta\rho_i^{opt} \tag{10}$$

In fact, it is difficult to update the density variable in the inner loop only depending on the incremental update scheme of the density variable Eq. (5). If a density variable update scheme is established, this problem can be easily solved. Therefore, PTO has designed the following density variable update scheme in Eq. (11).

$$\rho_i^{opt} = \rho_i^{pro} + \Delta\rho_i^{opt} \text{ .} \tag{11}$$

Where, $\rho_i^{pro}$ is the optimal density of the element. $V_{\mathrm{RM}}$ can be continuously used to update the density variable in the inner ring until the termination condition is met. The remaining material is not less than 0.001.

When the density variable update scheme updates the density variable in the inner ring, the density variable value of some elements may exceed the density range without density boundary. In order to avoid this phenomenon and ensure the normal implementation of the density variable update, mandatory measures must be taken to limit the element density within the boundary. See Eq. (12) for specific implementation measures.

$$\rho_i^{pro} = \begin{cases} \rho_{\min} & \rho_i^{opt} \le \rho_{\min}, \\ \rho_i^{opt} & \rho_{\max} < \rho_i^{opt} < \rho_{\min}, \\ \rho_{\max} & \rho_i^{opt} \ge \rho_{\max}. \end{cases} \tag{12}$$

Where, $\rho_i^{pro}$ is the optimization density variable obtained by each iteration in the inner loop.

### 3.4 Density Update Scheme in the Main Loop

The last step of the loop updates the element density by linearly mixing the element density (Eq.(13)) in the previous iteration and the optimized element density in the current iteration.

$$\rho_i\,(iter+1) = \alpha\rho_i\,(iter) + (1-\alpha)\rho_i^{pro} \text{ .} \tag{13}$$

Where $\rho_i\,(iter+1)$ is the density variable obtained at the (*iter*+1)-th iteration of the density variable update in the main loop. $\rho_i\,(iter)$ is the density variable obtained at the *iter*-th iteration, $\rho_i^{pro}$ is the element density in the internal iteration, $\alpha$ is the historical balance coefficient, which mainly reflects the dependence of the density variables of the two iterations. It indicates that the $\rho_i\,(iter+1)$ has a weak dependence on its previous iteration value $\rho_i\,(iter)$ when $\alpha$ is relatively small. It should be noted that, it is difficult to converge within 1000 iterations when $\alpha = 0$. The density variable does not play a role in the update process of the density variable in the main loop when $\alpha = 1$. So far, the PTO algorithm has experienced a complete cycle. If the maximum change of element density between two consecutive iterations is less than the specified tolerance of 0.001, the main cycle stops.

### 3.5 Steps and pseudocode of PTO algorithm

The execution flowchart of PTO algorithm is shown in Figure 1. Meanwhile, the pseudocode of PTO algorithm is shown in this section.

**Algorithm 1.** The Pseudo code of PTO algorithm

**Begin**

**Step1: Initialization.** Setup FE and tress analyses and Filter

**Step2: While**

$V_{TM}$ calculation with $V_{TM}=\begin{cases}\sum_{i=1}^{N}\rho_i v_i+0.001N & \max(\sigma_i)\le\sigma_{\lim t}\\ \sum_{i=1}^{N}\rho_i v_i-0.001N & \max(\sigma_i)\le\sigma_{\lim t}\end{cases}$

Perform FE and compliance analyses

Check stop criteria, break if satisfied

**Step3:** Run optimization algorithm

Set $V_{RM} = V_{TM}$

Until $V_{RM}$ is small enough

**Step4: while**

Distribute $V_{RM}$ to elements proportionally to $\Delta\rho_i^{opt}=V_{RM}\cdot\sigma_{pro}$

Apply filter

Apply density limits

Calculate actual material amount $V_{AM}$

Update $V_{RM} = V_{TM}–V_{AM}$

**End while**

**Step5:** Update density

$\rho_i(t+1)=\alpha\rho_i(t)+(1-\alpha)\rho_i^{opt}$

**End while**

**Step6: Return.** Return the optimal value.

**End**

## 4 Adaptive Enhanced Proportional Topology Optimization Algorithm

### 4.1 A new material interpolation model

The interpolation model proposed in Section 3.1 will have different interpolation curves depending on the penalty factor. For Eq. (3), Figure 2 shows several sets of interpolation curves with different parameters, material properties are input as 1 for Young's modulus $E_0$ , and $E_{\min}$ is a very small Young's modulus (usually $10^{-9}$). With the increase of *p*, the curve becomes steeper near point (1, 1), and tends to be stable near point (0, 0). In other words, when the element density is close to 0, the reduction rate of elastic modulus ( *E* ) is small. On the contrary, the increase rate of $E$ is large when the element density is close to 1. It is obvious that with the increase of *p*, the intermediate cell density value is converted to the two poles of the cell density value, which is obviously unscientific. Although most of the intermediate density are avoided, the final structure may be inaccurate if the intermediate density value is filtered out prematurely.

Based on the above analysis, in order to avoid the aforementioned drawback, this section uses a newly fitted logistic interpolation model (Zhang 2021), with the specific expression can be see Eq. (14).

$$E(\rho_i)=E_0*\exp^{\lambda\rho_i}/(\lambda\mu+\exp^{\lambda\rho_i})\quad \rho_i\in[0,1]\text{ ,} \tag{14}$$

Where, $\lambda$ is called threshold, $\mu$ is the correlation coefficient, $E$ is the density-related Young's modulus. In order to avoid the occurrence of singular stiffness matrix, $E_0=1$ is the Young's modulus of solid materials, and $E_{\min}$ is a very small Young's modulus (usually $10^{-9}$), $\rho_i$ is the density variable of the discrete element *i*. However, parameters $\lambda$ and $\mu$ have a significant impact on the interpolation model. Figure 4 shows the curve of the improved interpolation density model. The left graph of Figure 4 shows the family of curves corresponding to different $\lambda$ values with a fixed $\mu=3000$ , and the right graph shows the family of curves corresponding to different $\mu$ values with $\lambda=15$ .

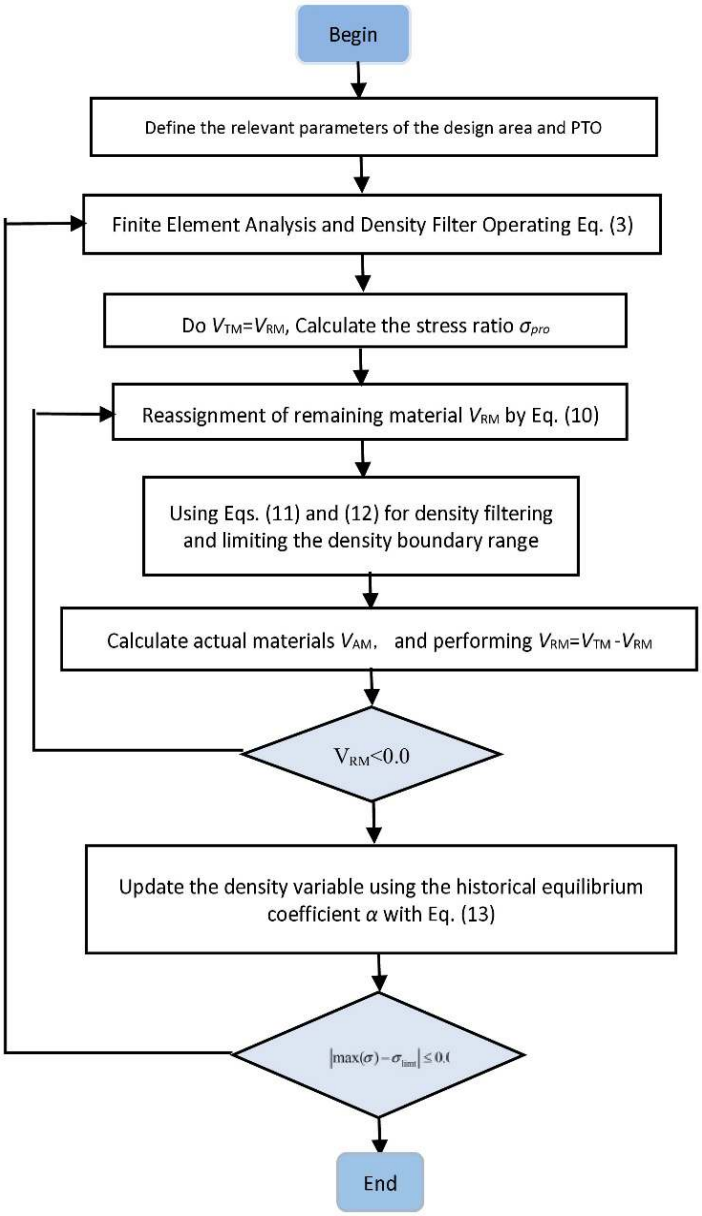



**Figure 1** The execution flowchart of PTO algorithm.

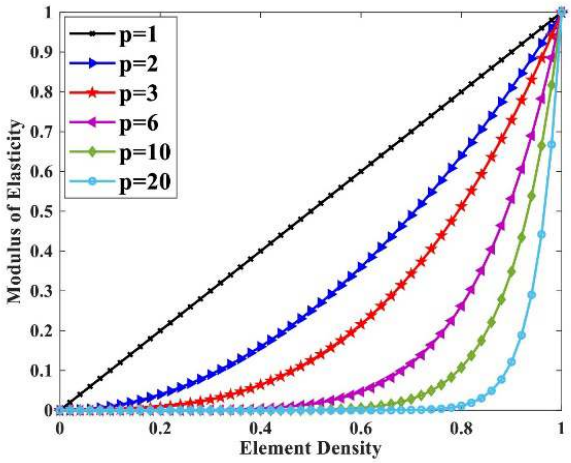



**Figure 2** Original interpolation model.

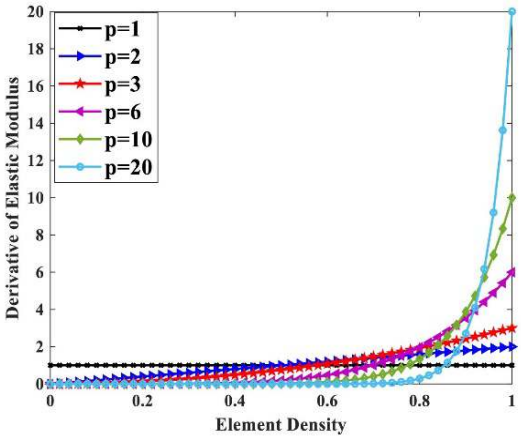



**Figure 3** Derivative of the original interpolation model.

As shown in Figure 2, the SIMP scheme removes too many high-density elements, which will affect the subsequent search of the optimal topology. Due to the large number of intermediate density, the optimal topology after punishment will inevitably produce a large number of gray elements. Figure 4 shows that this method can quickly polarize most elements to 0 or 1.0 with the same probability. Therefore, in the final topology, the number of elements with intermediate density will be sharply reduced, so as to obtain a topology design with obvious boundary. One of the most obvious differences between Figure 4 and the original interpolation model is that the new interpolation model takes the density value of 0.5 as the middle limit, punishes the density smaller than the middle limit to tend to 0, and the density larger than the middle limit to tend to 1, avoiding the detention of the middle density.

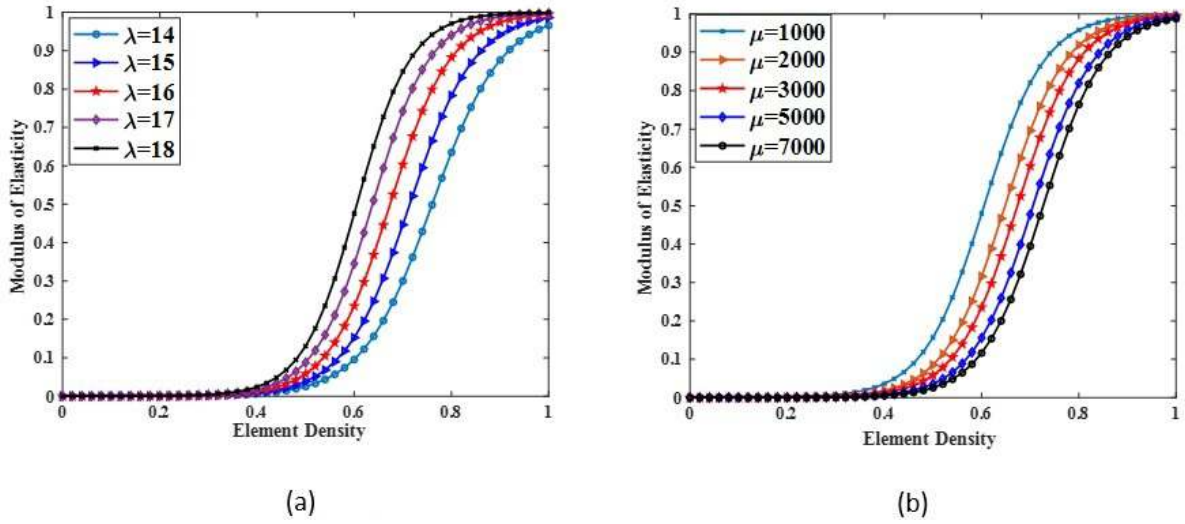



**Figure 4** Improved interpolation model.

To illustrate the superiority of this method, the sensitivity of the interpolation model in the original PTO method and the improved interpolation model in this paper is further analyzed, that is, the derivatives of the interpolation Eqs. (3) and (14), as shown in Figures 3 and 5 respectively. As can be seen from Figure 3, with the increase of penalty factors, the number of deleted elements gradually increases. Among them, most of the relative densities between 0.5 and 1.0 will tend towards 0 polarization iteration, which will inevitably affect the subsequent search for the optimal topology and make it difficult to ensure the accuracy of the calculation results. It can be seen from Figure 5 that the sensitivity curve of Young's modulus moves horizontally in improved interpolation model. No matter how the penalty factor changes, the sensitivity information of these elements is almost not 0. It is further explained that the improved method makes all elements in the design field beneficial to the whole process of topology optimization. Compared with $\mu$, $\lambda$ has a greater influence on the curve. The optimal topology can be obtained by setting different relative density dividing points for different engineering applications,.

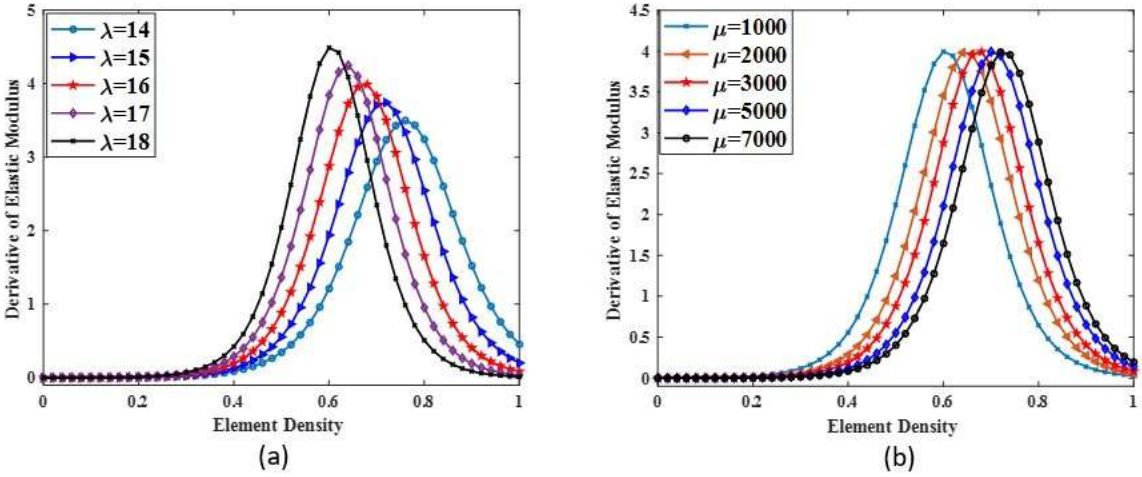



**Figure 5** Derivative of improved interpolation model.

### 4.2 Density filter parameters of Cauchy type

In the whole topological design process, the selection of the appropriate weighting coefficient $w_{ij}$ for the density filter Eq. (5) has a significant impact on the final topological results. The Cauchy distribution has a strong global development ability and can diversify the initial population. Therefore, the weighting function based on Cauchy distribution is as follows:

$$w_{ij} = 1/\pi r_0(1 + r_{ij}/r_0)\ . \tag{15}$$

Where, $r_{ij}$ is the distance between elements *i* and *j*, and $r_0$ is the filter radius. Compared with the original weight factor, the objective function may not get the optimal result, but to some extent, it can inhibit the appearance of the chessboard effect to a greater extent.

### 4.3 Update scheme of target material volume

The target material volume ($V_{\mathrm{TM}}$) and the remaining material volume($V_{\mathrm{RM}}$) are important intermediate variables for performing density variable updates, and different expressions can also have a significant impact on the convergence of the algorithm. In order to improve the convergence performance of the algorithm, slight modifications were made to the original target material volume formula based on the PTO algorithm. The specific expression is shown in Eq. (16).

$$V_{TM} = \begin{cases} \sum_{i=1}^{N} \rho_i v_i + 0.001(nelx * nely) & \max(\sigma_i) > \sigma_{\mathrm{limt}}, \\ \sum_{i=1}^{N} \rho_i v_i + \tau(nelx * nely) & \max(\sigma_i) \le \sigma_{\mathrm{limt}}, \\ \sum_{i=1}^{N} \rho_i v_i + 0.001(nelx * nely) & \max(\sigma_i) > \sigma_{\mathrm{limt}},\ \ iter < 50, \max(\sigma_{\mathrm{Iter}}(iter-4:iter)) > \sigma_{\mathrm{limt}}. \end{cases} \tag{16}$$

Where, $\sigma_{\mathrm{limt}}$ is the von Mises stress, $iter$ represents the current number of iterations, $\sigma_{\mathrm{iter}}$ represents the maximum von Mises stress generated in each iteration, and $nelx * nely$ is the total number of discrete elements, $\tau$ is a very small constant. In this article, let $\tau = 10^{-8}$, it is to ensure the normal updating of the target material volume, in order to prevent the algorithm from not converging due to the continuous exceeding of the stress limit by the maximum von Mises stress of the elements (Cheng et al. 2021).

### 4.4 Arctangent density update strategy

In topology optimization, hybrid projection operators are commonly used to improve the optimization results. For example, Xu et al. (2010) utilized a volume preserving density filter based on Heaviside type projection operator to

promote a more discrete density variable, even if the density variable is closer to the 0/1 solution. Wang et al. (2011) used an improved transparent type projection operator to alleviate the poor convergence caused by volume preservation issues. Li and Khandelwal (2015) solved the structural optimization problem of obtaining binary discrete topology by combining the volume preserving Hivi type projection operator and filter. To enhance the stability of the iterative process, this section adopts an arctangent-based density filtering function derived from the Heaviside function to further filter the density variables. This method enables the attainment of 0/1 topology optimization results while improving the smoothness of the iterative process. It also ensures that a greater number of highly correlated density elements continuously participate in the iteration, thereby facilitating the search for the optimal topology optimization result. The expression of its function (Bendsoe and Kikuchi 1988) is as follows:

$$\overline{\rho}_i = \left(\arctan(\eta\theta) + \arctan(\eta(\rho_i - \theta))\right) / \left(\arctan(\eta\theta) + \arctan(\eta(1-\theta))\right). \tag{17}$$

Where, $\theta$ is defined as the density threshold, $\theta \in [0,1]$, and $\rho_i$ is the unit density value after density filtering. $\overline{\rho_i}$ represents the unit density value after Heaviside bidirectional threshold density filtering. This article emphasizes that $\eta$ in the equation is an adaptive positive number that controls the penalty rate. For different $\alpha$ and proportional exponents $q$, it can be obtained using the intelligent algorithm. The model to be optimized is as follows:

$$\begin{aligned} &\text{find} \quad \min \quad V(\overline{\rho}) = \sum_{i=1}^{N} \overline{\rho}_i v_i \\ &\text{s.t} \begin{cases} \mathbf{KU} = \mathbf{F} \\ \sigma_i \le \sigma_{\text{limt}}, if \quad \rho > 0, \\ 0 \le \rho_{\min} \le \rho_i \le \rho_{\max} \le 1, \\ \overline{\rho}_i = \left(\arctan(\eta\theta) + \arctan(\eta(\rho_i - \theta))\right) / \left(\arctan(\eta\theta) + \arctan(\eta(1-\theta))\right). \end{cases} \end{aligned} \tag{18}$$

Figure 6 shows the influence of different parameters $\eta$ on density filtration when θ=0.5. It is evident that as $\eta$ continues to increasing, the density values also tend towards 0 or 1, with the middle density tending towards both ends. Meanwhile, as the value of $\eta$ gradually increases, the density filtering function in arctangent form filters more slowly and steadily, allowing more intermediate density values to participate in the iterative process and further improve the calculation accuracy. Note that the arctangent function equals 0 at the point of 0, which would render the function curve non-representable. Therefore, a relatively small value of $\eta$ should be set.

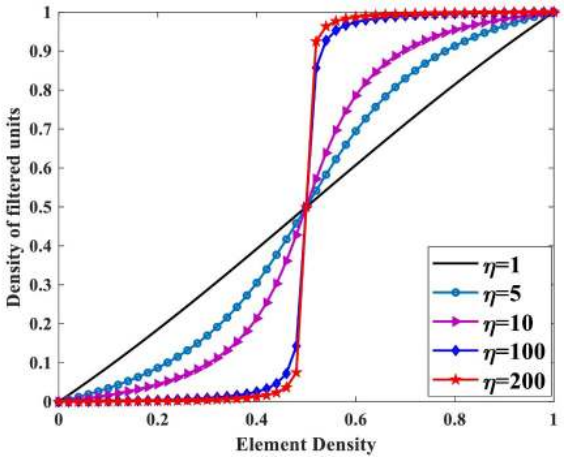



**Figure 6** The effect of different parameters $\eta$ on density filtration.

In order to avoid the intermediate density units that are equal to the threshold being ignored in the penalty, the threshold is dynamically updated in an iterative manner in this paper. The initial value is taken as 0.5 from the binary method in the [0,1] interval, then the threshold $\theta$ is dynamically updated using the binary method of the maximum and minimum values of the current density. The specific mathematical expression is shown in Eq. (19).

$$\theta = \max(\rho(iter)) + \min(\rho(iter))/2. \tag{19}$$

### 4.5 Dynamic adaptive historical balance coefficient

There is a parameter called the historical balance coefficient $\alpha$ in the density Eq. (13), which mainly reflects the dependency degree between the density variables of two consecutive iterations. It linearly blends the optimization results of the current and previous iterations to achieve a stable solution process and obtain the optimal design result. The updated element density value is defined as the sum of half of the density value from the previous iteration and half of the density value obtained through proportional allocation in the current iteration when $\alpha = 0.5$. The density variable has no effect on the density variable update process in the main loop when $\alpha = 1$. The equation indicates that the selection of the historical balance coefficient $\alpha$ has a significant impact on the PTO algorithm. Therefore, selecting an optimal historical balance coefficient $\alpha$ is a problem worthy of in-depth consideration by researchers.

The data shows that the objective function and iteration times are low, and the algorithm is stable when the historical balance coefficient $\alpha = 0.5$. When $\alpha < 0.5$, there may be some numerical instability during the optimization process; When $\alpha > 0.5$, the number of iterations gradually increases. Based on the above analysis, this paper introduces an adaptive dynamic historical balance coefficient method to improve the accuracy and optimization efficiency of PTO. The mathematical model of the specific dynamic historical balance coefficient scheme is shown in Eqs. (21) and (20).

$$\alpha = \alpha + step * h(iter), \tag{20}$$

$$h(t) = 1\text{-}\exp^{(iter/Maxiter)} / (\exp\text{-}1). \tag{21}$$

Where, $h(iter)$ represents the adaptive dynamic parameter related to the number of iterations, and *Maxiter* is the maximum number of iterations. When the balance historical coefficient $\alpha$ in the density update formula is 0, the algorithm may not converge within 1000 iterations, so the maximum number of iterations (*Maxiter*) is taken as 1000. *step* represents the proportional coefficient of the weight, $step \in [0.001,\ 0.003]$. An excessively small value of α may lead to numerical instability, while an excessively large historical balance coefficient will cause the optimization result of the current iteration to be strongly dependent on the design variable values obtained from the previous iteration and reduce the optimization efficiency. To maintain the stability of the algorithm and avoid unpredictable situations, upper and lower bounds are imposed on the historical balance coefficient, such that $\alpha \in [0,\ 0.5]$. In addition, Eq. (20) is only valid when certain conditions are satisfied, which are specified as follows:

$$\max(\rho(iter+1) - \rho(iter)) \le \rho_{\text{toler}}(iter), \tag{22}$$

$$\rho_{\text{toler}}(iter+1) = \omega(\max(\rho_{\text{toler}}(iter),\ 0.001)). \tag{23}$$

Where, $\rho_{\text{toler}}(iter)$ is the adjustment tolerance, and the initial tolerance $\rho_{\text{toler}}(0)$ is taken as 0.2. $\omega$ represents the scaling factor, through which the adjustment tolerance value gradually decreases as the balance factor increases. Here, it is worth noting that these parameter values can be adjusted appropriately according to specific engineering problems. The dynamic historical balance coefficient can reduce the number of iterations for the same problem and parameters, thereby improving the optimization efficiency of PTO algorithm. In addition, lower flexibility values were obtained while avoiding numerical instability during the optimization process.

### 4.6 Steps and Convergence Analysis of adaptive enhanced PTO algorithm (AEPTO)

Combining the improved interpolation model, Cauchy density filter parameters, arctangent density update strategy and dynamic adaptive balance coefficient PTO algorithm, an improved version of PTO algorithm is obtained, which can not only improve the efficiency of algorithm optimization but also improve the accuracy of the algorithm, and can reduce the generation of gray units in the final optimization results to a certain extent. In addition, since the improved version of proportional topology optimization does not require gradient information and combines the bionic meta-heuristic intelligent algorithm, it can also be called an intelligent algorithm with specific topology optimization. The specific process steps of the algorithm are shown in Figure 7.

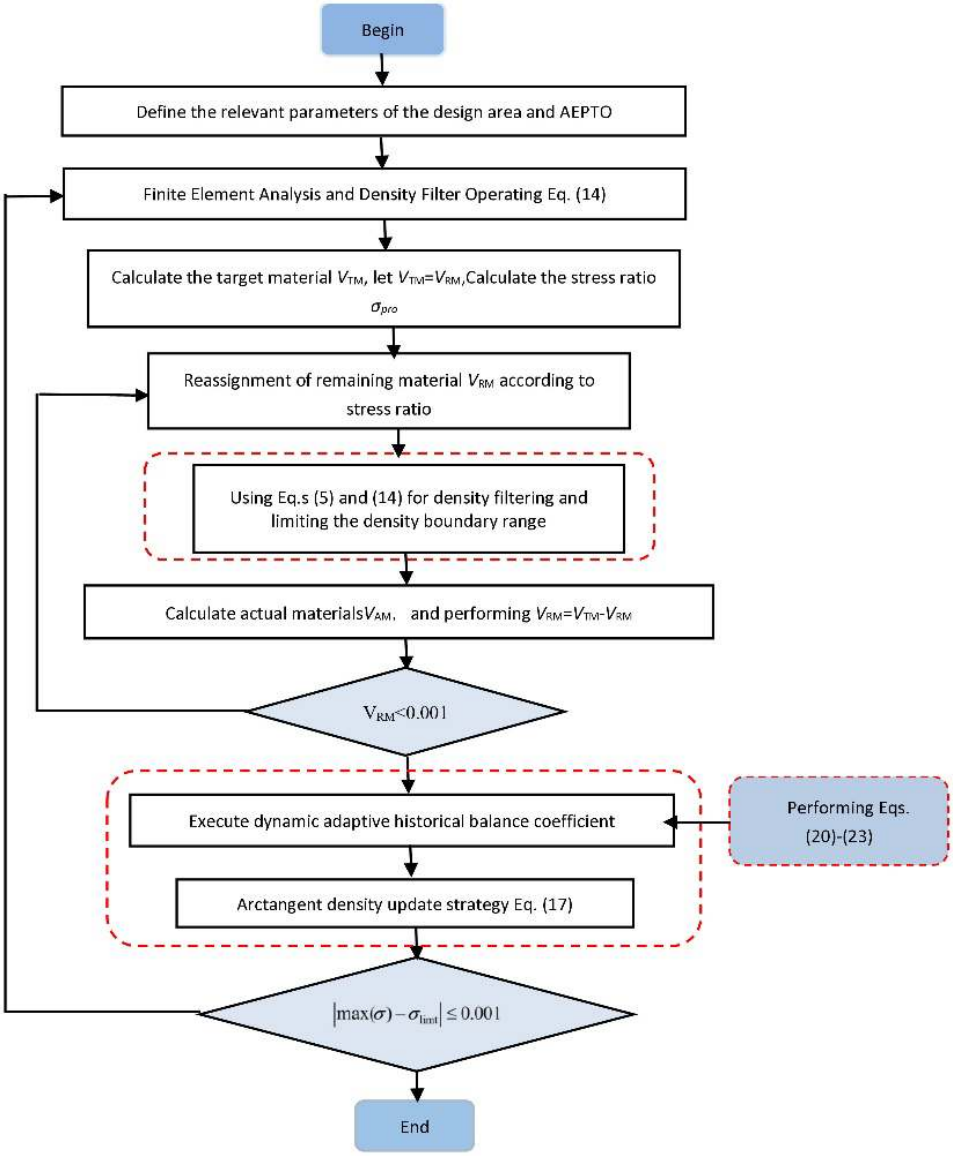



**Figure 7** The execution flow chart of AEPTO algorithm .

To ensure the theoretical completeness and engineering practicality of the AEPTO algorithm, this section systematically analyzes its convergence, computational complexity.

In each iteration, the AEPTO algorithm updates the density variables through proportional allocation, filtering, projection, and dynamic balance coefficient adjustment. Its iterative process can be regarded as a nonlinear mapping:

$$\rho(k+1)=\Gamma(\rho(k)). \tag{24}$$

Where, $\Gamma$ denotes a complete AEPTO iterative process. The input is the density variable vector $\rho(k)\in[0,1]$ at the *k*-th iteration, and the output is the optimized density variable vector $\rho(k+1)\in[0,1]$ at the (*k*+1)-th iteration.

Under fixed parameter rules, AEPTO can stably converge to the minimum-volume topological structure that satisfies stress constraints for three reasons: First, the iterative process is a smooth and bounded mapping, Cauchy filtering and arctangent projection ensure that the density update is continuous without abrupt changes, and all density values are always confined within the range of 0 (void) to 1 (solid), thus avoiding abnormal fluctuations. Second, the objective (volume fraction) is monotonically decreasing. In each iteration, rational material allocation and density polarization (reduction of intermediate gray-scale elements) ensure that the structural volume only decreases or remains unchanged rather than rebounding.Third, the volume has a clear lower bound. To satisfy stress safety and the minimum structural stiffness requirements, the volume cannot decrease infinitely and has a minimum critical value.

According to the fundamental mathematical principle that "a monotonically decreasing sequence with a lower bound must converge", the volume fraction of the AEPTO algorithm will gradually approach this minimum critical value, and the density distribution will stabilize to the optimal state, ultimately converging to the required topological structure.

Subsequent numerical examples will further illustrate the numerical convergence, presenting the variation curves of volume fraction with the number of iterations under typical parameter settings. It can be observed that the volume fraction of AEPTO drops rapidly in the initial stage of iteration, tends to stabilize in the middle stage, and finally converges to a steady solution without obvious oscillations, which indicates that the algorithm has favorable numerical stability.

The computational cost of a single iteration of AEPTO algorithm mainly stems from finite element analysis (FEA), stress calculation and proportional allocation, Cauchy filtering, arctangent projection, and dynamic equilibrium coefficient updating. Its total complexity is approximately $O(n*m)$ (where $n$ is the number of elements and $m$ is the number of iterations), which is comparable to that of PTO algorithm. However, due to the introduction of projection and dynamic mechanisms, the actual number of iterations is significantly reduced, thus achieving an advantage in overall computational time.

## 5 Application of the adaptive enhanced proportional topology optimization algorithm

Cantilever beams, L-shaped beams, and MBB beams are widely used in engineering applications. Cantilever beams are employed in aero-engine blades and robotic arms, L-shaped beams find application in corner brackets of automobile chassis and joints of building steel structures, and MBB beams are utilized in crossbeams of sea-crossing bridges and supporting beams of high-speed railway tracks. Therefore, these three typical beam structures are taken as the optimization objects to solve the minimum volume problem under constraints including stress constraints, displacement constraints, and various force loads. A comparison is also made with the PTO algorithm, which verifies the effectiveness and superiority of AEPTO algorithm. The material properties are shown in Table 1.

**Table 1** Material properties.

| Material properties | Young's modulus | filter radius | minimum Young's modulus | Poisson's ratio | penalty coefficient |
|---|---|---|---|---|---|
| | ($E_0$) | ($r_0$) | ($E_{min}$) | (υ) | ($p$) |
| Parameter Value | 1 | 1.5 | $1.0\times10^{-9}$ | 0.3 | 3 |

### 5.1 Evaluating indicator

The performance of any algorithm needs to be evaluated through certain criteria. Therefore, this section presents the evaluation metrics used by the PTO and AEPTO algorithms to verify their effectiveness and superiority, including the Contrast Index ( $C_{\text{index}}$ ), Gray Element Index ( $G_{\text{index}}$ ), number of iterations (*Iter*), topology structure, and material volume fraction of the optimized structure. Flexibility and the number of iterations can reflect the algorithm's global optimization capability and convergence performance. In summary, the smaller the material volume fraction and the number of iterations, the stronger the global optimization ability and the better the convergence performance. The topological structure is adopted to reflect the effect of the optimized structure. Generally speaking, an optimized structure can be regarded as satisfactory if it has a clear outline and no redundancy.

The comparison index ( $C_{\text{index}}$ ) is used to measure the algorithm's ability to approximate the density variable to 0/1, that is, its ability to obtain black and white structures. The larger the $C_{\text{index}}$ value is, the stronger the algorithm's capability to approximate density variables to 0/1, and the clearer the outline of the optimized structure will be. The larger the $C_{\text{index}}$ the stronger the algorithm's ability to approximate the density variable to 0/1, and the clearer the optimized structural contour. The calculation method of $C_{\text{index}}$ (Biyikli and To 2015) can be written as:

$$C_{\text{index}} = \left(Num(\rho_i < 0.01) \text{ or } Num(\rho_i > 0.99)\right) / SumNum. \tag{25}$$

In Eq. (25), $N_{\text{um}}$ denotes the total number of elements and $\rho_i$ is the density of elements.

The gray-scale element index ( $G_{\text{index}}$ ) is used to measure the proportion of grayscale elements (intermediate density interpolation materials) in the optimized structure. Usually, the larger the $G_{\text{index}}$ , the more grayscale elements exist in the optimized structure. The calculation formula of $G_{\text{index}}$ is as follows:

$$G_{\text{index}} = \left(N_{um}(\rho_i \geq 0.01) \text{ and } N_{um}(\rho_i \leq 0.99)\right) / SumNum \ . \tag{26}$$

In order to measure the degree of dispersion of topological configurations, that is, to determine whether the optimization solution obtained is a discrete solution, a discrete index (2001) is adopted, which is in the form of Eq. (27):

$$M_{\text{nd}} = \left( \sum_{i=1}^{N} 4\rho_i(1-\rho_i) \right) \Big/ N \times 100\%. \tag{27}$$

This function exhibits a parabolic form. If the density distribution is completely discrete (i.e., all densities are either 0 or 1), then $M_{\text{nd}}$=0. If the entire design consists entirely of gray-scale elements (i.e., assuming all densities equal 0.5), then $M_{\text{nd}}$=1. $M_{\text{nd}}$ is a discreteness index, the smaller the value of this index, the better the discreteness, and the clearer the topological configuration.

### 5.2 Ablation Study-Analysis of the Independent Contributions of Each Improved Component

To further verify the independent roles of each improved module in the adaptive enhanced proportional topology optimization algorithm (AEPTO) proposed in this paper, a systematic ablation study is designed in this section. By comparing the optimization performance under different module combinations on a cantilever beam example, the contributions of each technical component to the algorithm's convergence, structural clarity, and lightweight effect are clarified.

The experiment takes a cantilever beam (Figure 8) as the object, with the same material and boundary conditions as those in Section 5.1. The design domain is discretized into 120×60 four-node quadrilateral elements, and the stress constraint is set as $\sigma_{\text{limt}} = 0.57$. The following six algorithm configurations are compared in Table 2.

**Table 2** Ablation Algorithm Configurations.

| Configuration | Interpolation Model | Density Filter | Projection Strategy | Historical Balance Coefficient | Abbreviation |
|---|---|---|---|---|---|
| ① | SIMP | Conic Filter | None | Fixed $\alpha$=0.5 | PTO |
| ② | Logistic | Conic Filter | None | Fixed $\alpha$=0.5 | PTO-Log |
| ③ | SIMP | Cauchy Filter | None | Fixed $\alpha$=0.5 | PTO-Cauchy |
| ④ | SIMP | Conic Filter | None | Dynamic $\alpha$ | PTO-Dynα |
| ⑤ | SIMP | Conic Filter | Arctangent Projection | Dynamic $\alpha$ | PTO-Arctan-Dynα |
| ⑥ | Logistic | Cauchy Filter | Arctangent Projection | Dynamic $\alpha$ | AEPTO |

The remaining parameters are unified as follows: $q = 2.5, \eta = 2.8$ (if Arctangent Projection is used), $\lambda = 15, \mu = 3000$ (for the Logistic model).Table 3 presents the comparison of optimization results of the six configurations on the cantilever beam problem.

**Table 3** The comparison of optimization results of the six configurations on the cantilever beam problem.

| Configuration | Volume Fraction( *V*) | Number of Iterations (*Iter*) | $C_{\text{index}}$ | $G_{\text{index}}$ | $M_{\text{nd}}$ |
|---|---|---|---|---|---|
| ① PTO | 0.34 | 320 | 0.8869 | 0.1131 | 0.0696 |
| ② PTO-Log | 0.33 | 356 | 0.8494 | 0.1506 | 0.0879 |
| ③ PTO-Cauchy | 0.35 | 302 | 0.8708 | 0.1292 | 0.0813 |
| ④PTO-Dynα | 0.34 | 409 | 0.8867 | 0.1133 | 0.0696 |
| ⑤PTO-Arctan-Dynα | 0.29 | 141 | 0.8306 | 0.1694 | 0.0839 |
| ⑥ **AEPTO** | 0.27 | 137 | 0.8233 | 0.1694 | 0.0859 |

As can be seen from the above table, compared with Configuration ①, the Logistic interpolation model (Configuration ②) shows a slight decrease in volume fraction and a slight increase in gray-scale elements. This indicates that it can more effectively push materials toward the two ends (0/1) and enhance the lightweight effect, but may sacrifice partial discreteness. For the Cauchy filter (Configuration ③), there is a slight improvement in structural clarity ($C_{\text{index}}$) and a smoother convergence curve. This demonstrates that it helps suppress numerical oscillations and improve optimization

stability, but the volume fraction increases instead. Regarding the dynamic historical balance coefficient (Configuration ⑤), the number of iterations decreases significantly with a slight increase in gray-scale elements, indicating that it can more effectively push materials toward the two ends. For the combination of dynamic historical balance coefficient and Arctangent projection (Configuration ④), the number of iterations is remarkably reduced, achieving the fastest convergence speed. This proves that the adaptive mechanism can effectively improve algorithm efficiency.

AEPTO (Configuration ⑥) achieves the optimal volume fraction (0.27), which is approximately 34.1% lower than that of the original PTO, and strikes a good balance between the number of iterations, structural clarity, and discreteness. This indicates that there is a synergistic effect among the improved modules: the Logistic model and Arctangent projection jointly promote the polarization of density toward 0/1, the Cauchy filter enhances global exploration capability and avoids premature convergence, the dynamic α mechanism accelerates convergence and improves robustness.

The following conclusions can be drawn from the ablation study: the Logistic interpolation model is the core for enhancing the lightweight effect, the Arctangent projection and dynamic α mechanism collectively improve convergence speed and stability, the Cauchy filter strengthens the algorithm's robustness and structural clarity.

The combination of the four modules exerts a synergistic effect in AEPTO, outperforming single-module improvements or the original PTO in terms of lightweight performance, convergence, and structural discreteness.

This experiment verifies the effectiveness and necessity of each improved component in AEPTO at the module level, providing further support for its engineering applicability.

### 5.3 Cantilever beam problem

Figure 8 shows the structural diagram of the cantilever beam. The material properties are listed in Table 1. The ratio of length, width and thickness in the design area is equal to 120:60:1. The boundary range of the density variable is [0, 1]. The number of elements for the external load is set to 3, and the stress ratio influence coefficient *q* is in the range of 2 *to* 2.75. The design domain is discretized into a 120×60 (*nelx*×*nely*) bilinear quadrilateral element. The cantilever beam is fixed at the left boundary in both *x* and *y* dimensions, and a shear force F=1 is applied at the middle of the right boundary. The numbering of nodes and units is standardized from top to bottom and from left to right. In addition to the basic parameters, other parameters used by the algorithm need to be set separately according to the requirements of the examples and the research needs of the problem.

In the cantilever beam, the control parameters for the optimization problem are set as follows: *q* is varied from 2 to 2.75 with an increment of 0.25, and $\alpha \in [0,1]$. Herein, since an excessively large value of $\alpha$ leads to an increase in the number of convergence iterations and an over-reliance on the accumulated optimal volume fraction from the inner loop, $\alpha$ is varied from 0 to 0.5 with an increment of 0.1. The final optimal topology index results of the cantilever beam obtained by setting the optimal control parameters for PTO and AEPTO algorithms are shown in Table 4. *V* represents the material volume fraction used to reflect the optimized structure, and *Iter*, $M_{nd}$, $C_{index}$ and $G_{index}$ can refer to the section 5.1. $\eta$ represents a positive adaptive control rate parameter in AEPTO, please refer to section 4.4 for details. Figures 9 and 10 respectively show the optimal topology results obtained by PTO and AEPTO algorithm with different *q* under different *α*. Figures 9 (a)- (f) correspond to the final optimal topology results of PTO with $\alpha$ values of 0, 0.1, 0.2, 0.3, 0.4, and 0.5, respectively. Figure 10 (a)- (f) correspond to the final optimal topology results of AEPTO when α is set to 0, 0.1, 0.2, 0.3, 0.4, and 0.5, respectively. The bold emphasis in Table 4 highlights the better algorithm results among the two algorithms with the same $\alpha$ and $\eta$, and the underlined data represents the best results corresponding to each algorithm under the same $\alpha$.

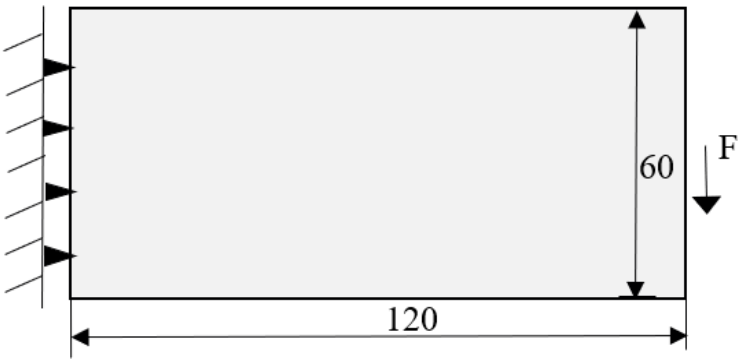



**Figure 8** Schematic Diagram of Cantilever Beam.

**Table 4** Optimization results of cantilever beam obtained by PTO and AEPTO algorithm considering control parameter setting.

| Evaluation metric | | Algorithms | | | | | | | |
|---|---|---|---|---|---|---|---|---|---|
| | | PTO | AEPTO | PTO | AEPTO | PTO | AEPTO | PTO | AEPTO |
| **α** | **q** | **2** | | **2.25** | | **2.5** | | **2.75** | |
| 0 | V | 0.34 | **0.25** | 0.29 | **0.19** | 0.30 | **0.26** | 0.30 | **0.27** |
| | Iter | 164 | **97** | 220 | **217** | 202 | **121** | 208 | **225** |
| | $M_{nd}$ | 0.0697 | 0.1009 | 0.0996 | **0.0885** | 0.0961 | 0.1166 | 0.1030 | 0.1290 |
| | $C_{index}$ | 0.8822 | 0.8225 | 0.8308 | **0.8544** | 0.8378 | 0.8019 | 0.8281 | 0.8008 |
| | $G_{index}$ | 0.1178 | 0.1775 | 0.1692 | **0.1456** | 0.1622 | 0.1981 | 0.1719 | 0.1992 |
| | $\eta$ | / | 2.1 | / | 1.0 | / | 1.6 | / | 0.5 |
| 0.1 | V | 0.35 | **0.21** | 0.34 | **0.23** | 0.29 | **0.26** | 0.30 | **0.25** |
| | Iter | 174 | **128** | 182 | **118** | 240 | **111** | 230 | **177** |
| | $M_{nd}$ | 0.0700 | 0.0805 | 0.0694 | 0.1026 | 0.0984 | 0.1019 | 0.0959 | 0.1244 |
| | $C_{index}$ | 0.8861 | 0.8583 | 0.8844 | 0.8247 | 0.8322 | 0.8083 | 0.8378 | 0.7981 |
| | $G_{index}$ | 0.1139 | 0.1417 | 0.1156 | 0.1753 | 0.1678 | 0.1917 | 0.1622 | 0.1919 |
| | $\eta$ | / | 2.1 | / | 2.1 | / | 2.1 | / | 1.1 |
| 0.2 | V | 0.35 | **0.18** | 0.34 | **0.19** | 0.34 | **0.19** | 0.33 | **0.27** |
| | Iter | 195 | **180** | 198 | **208** | 201 | **154** | 218 | **245** |
| | $M_{nd}$ | 0.0700 | 0.0782 | 0.0695 | 0.0828 | 0.0687 | 0.0795 | 0.0686 | 0.1296 |
| | $C_{index}$ | 0.8861 | 0.8639 | 0.8861 | 0.8661 | 0.8864 | 0.8614 | 0.8878 | 0.7942 |
| | $G_{index}$ | 0.1139 | 0.1361 | 0.1139 | 0.1339 | 0.1136 | 0.1386 | 0.1122 | 0.2058 |
| | $\eta$ | / | 1.9 | / | 1.5 | / | 2.0 | / | 0.6 |
| 0.3 | V | 0.36 | **0.27** | 0.35 | **0.25** | 0.37 | **0.25** | 0.34 | **0.19** |
| | Iter | 209 | **102** | 223 | **118** | 227 | **141** | 238 | **226** |
| | $M_{nd}$ | 0.0701 | 0.0900 | 0.0695 | 0.0965 | 0.0692 | 0.1045 | 0.0690 | 0.0848 |
| | $C_{index}$ | 0.8833 | 0.8297 | 0.8861 | 0.8189 | 0.8864 | 0.8169 | 0.8886 | 0.8556 |
| | $G_{index}$ | 0.1167 | 0.1703 | 0.1139 | 0.1811 | 0.1136 | 0.1831 | 0.1114 | 0.1444 |
| | $\eta$ | / | 2.5 | / | 2.3 | / | 1.9 | / | 1.5 |
| 0.4 | V | 0.36 | **0.28** | 0.34 | **0.26** | 0.34 | **0.18** | 0.34 | **0.25** |
| | Iter | 242 | **109** | 261 | **122** | 266 | **170** | 274 | **144** |
| | $M_{nd}$ | 0.0698 | 0.0814 | 0.0698 | 0.0888 | 0.0695 | 0.0705 | 0.0689 | 0.0990 |
| | $C_{index}$ | 0.8842 | 0.8294 | 0.8861 | 0.8250 | 0.8864 | 0.8644 | 0.8886 | 0.8194 |
| | $G_{index}$ | 0.1158 | 0.1706 | 0.1139 | 0.1750 | 0.1136 | 0.1356 | 0.1114 | 0.1806 |
| | $\eta$ | / | 2.6 | / | 2.6 | / | 2.7 | / | 2.3 |
| 0.5 | V | 0.35 | **0.33** | 0.34 | **0.28** | 0.34 | **0.27** | 0.35 | **0.27** |
| | Iter | 292 | **95** | 314 | **134** | 320 | **137** | 298 | **158** |
| | $M_{nd}$ | 0.0699 | 0.0667 | 0.0699 | 0.0763 | 0.0696 | 0.0859 | 0.0683 | 0.0917 |
| | $C_{index}$ | 0.8853 | 0.8622 | 0.8867 | 0.8261 | 0.8869 | 0.8233 | 0.8869 | 0.8194 |
| | $G_{index}$ | 0.1147 | 0.1378 | 0.1133 | 0.1739 | 0.1131 | 0.1694 | 0.1131 | 0.1806 |
| | $\eta$ | / | 2.1 | / | 3.4 | / | 2.8 | / | 2.5 |

As can be seen from the data in Table 4, for any different values of $\alpha$ and $\eta$, AEPTO algorithm can effectively solve for the minimum volume of the cantilever beam in the stress-constrained optimization problem under the constraint of a maximum von Mises stress of 0.57. AEPTO can achieve the minimum material volume fraction and therefore the minimum material mass, thus achieving the goal of lightweighting. Under the same parameters, when $q\in$ [2, 2.75] and $\alpha$ are set to 0, 0.1, 0.2, 0.3, 0.4, and 0.5, the best results obtained by the PTO algorithm are 0.29, 0.29, 0.33, 0.34, 0.34, and 0.34, respectively. The best results obtained by the AEPTO algorithm are 0.19, 0.21, 0.18, 0.19, 0.18, and 0.27, with reductions of 34.5%, 27.6%, 45.5%, 44.1%, 47.1%, and 20.6%, respectively. Although most of the comparison indicators, grayscale indicators, and discrete indicators of the AEPTO algorithm are not as good as the original PTO algorithm, the results obtained by both algorithms may be somewhat difficult in beam manufacturing, and the difficulty of AEPTO is

relatively high. However, in terms of manufacturing, it is relatively difficult to produce accurate topological structures regardless of the amount of grayscale. However, it can be seen that the AEPTO algorithm is significantly better than the PTO algorithm in terms of iteration times when solving the optimization problem shown in Figure 8. From the perspective of lightweighting, the algorithm proposed in this paper can achieve better topological structures, higher utilization of material volume, material savings, and further reduce costs.

Based on the topological structures of each algorithm presented in Figures 9(c) and 10(c), differences can be observed between the two optimal topological structures obtained by the PTO and AEPTO algorithms. However, the structural frameworks are identical, with only minor differences in their dimensions. Furthermore, by examining the stress contours of optimized structures, it can be observed that although the stress distribution of the optimized structure obtained by the AEPTO algorithm is higher than that from the PTO algorithm, the stress within these regions remains within the allowable stress range, which indicates that both optimized structures are safe and reliable. According to the stress diagram, the score results of the optimized structure show that the best optimized structure obtained by AEPTO algorithm is superior to that obtained by PTO algorithm in terms of strength to weight ratio.

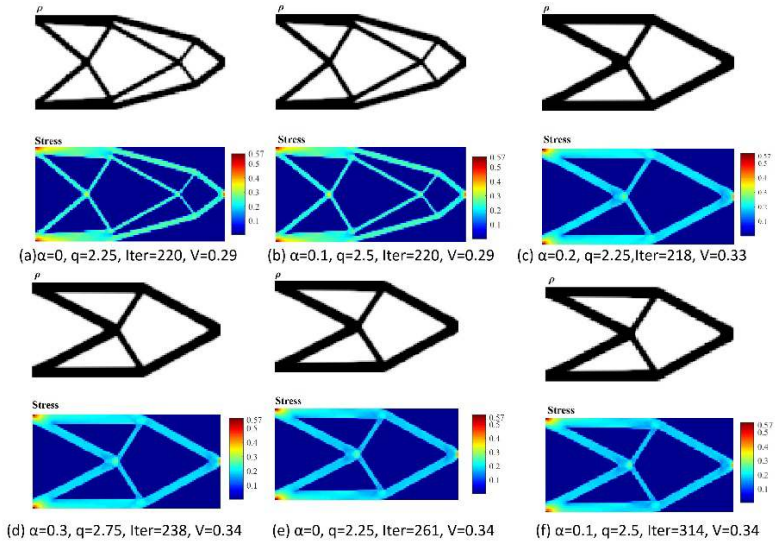



**Figure 9** Optimal Topological Structure of cantilever beam obtained by PTO algorithm.

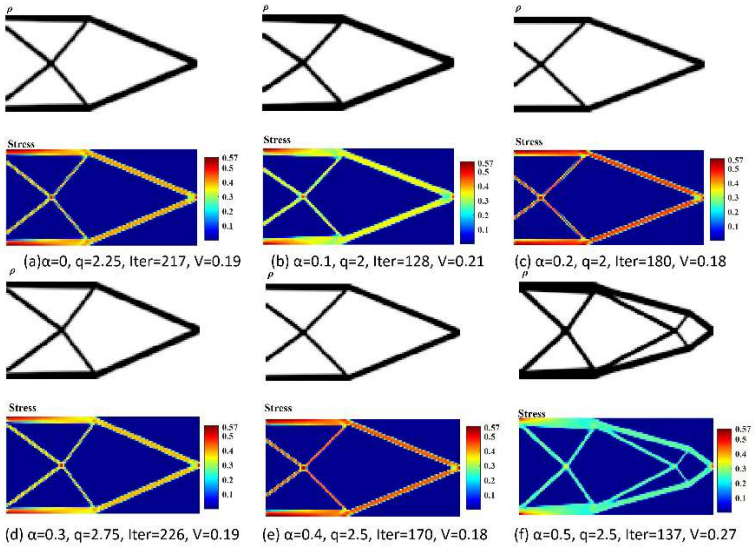



**Figure 10** Optimal Topological Structure of cantilever beam obtained by AEPTO algorithm.

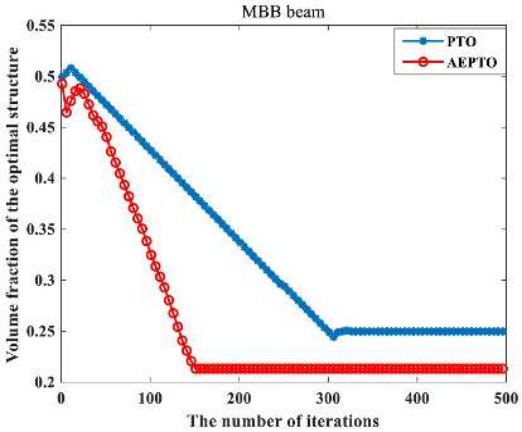



**Figure 11** Volume fraction convergence diagram of cantilever beam optimal topology obtained by PTO and AEPTO algorithms.

Figure 11 shows the iteration history curves of the optimal objective function for each algorithm. Under the same constraints, AEPTO algorithm achieved essentially the same optimization results with fewer iterations, improving the efficiency of the algorithm compared to PTO algorithm.

In summary, when solving the problem of the minimum-volume topological design of a cantilever beam under stress constraints, AEPTO algorithm is significantly superior to the original PTO algorithm in terms of lightweight performance and convergence. The introduction of a Cauchy-type filter, an arctangent-based density update strategy, and a dynamic historical balance coefficient has enhanced the new algorithm's ability to obtain accurate solutions, improved the topological structures, and increased its convergence speed. This enables the algorithm to save more material and achieve the goal of lightweight design.

### 5.4 L beam problem

The second example is the problem of a typical L-shaped beam, where the ratio of length, width, and thickness within the design area is 100:40:1, as shown in Figure 12. The L-shaped beam is discretized into 100 and 40 equal parts by the long (l) and short (s) sides, respectively. The L-shaped beam is fixed in both the $x$ and $y$ dimensions at the upper edge, and a normal force F=1 is applied at the top of the rightmost edge. The material properties are listed in Table 1. The boundary range of the density variable is [0,1]. The discrete element is a bilinear four node quadrilateral, with nodes and elements numbered uniformly in the order of top to bottom and left to right. In addition to the basic parameters, other parameters used by the algorithm also need to be separately set according to the requirements of the example and the research needs of the problem.

In L-shaped beam, the control parameters for the optimization problem are set to $q$ values ranging from 1.5 to 2.25 in increments of 0.25, $\alpha \in [0, 1]$, Here, due to excessive α leading to an increase in convergence times and excessive reliance on the optimal volume fraction accumulated by internal circulation, the value of $\alpha$ increases by 0.1 from 0 to 0.5. The final optimal topology index results of the L-beam obtained by setting the optimal control parameters for PTO and AEPTO algorithms are shown in Table 5. The meanings of the parameters and representation methods in the table are the same as those in Section 5.2. Figures 13 and 14 respectively show the optimal topology results obtained by PTO algorithm and AEPTO algorithm with different $q$ under different $\alpha$. Figure 13 (a) to (f) correspond to the final optimal topology results of PTO when α takes the values of 0, 0.1, 0.2, 0.3, 0.4 and 0.5, respectively. Figure 14 (a) to (f) correspond to the final optimal topology results of AEPTO when $\alpha$ is set to 0, 0.1, 0.2, 0.3, 0.4, and 0.5, respectively.

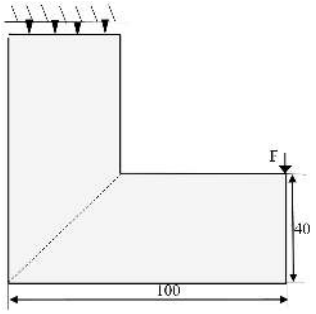



**Figure 12** Schematic Diagram of L Beam.

**Table 5** Optimization results of L beam obtained by PTO and AEPTO algorithm considering control parameter setting.

| Evaluation metric | | Algorithms | | | | | | | |
|---|---|---|---|---|---|---|---|---|---|
| | | PTO | AEPTO | PTO | AEPTO | PTO | AEPTO | PTO | AEPTO |
| $\alpha$ | $q$ | 1.5 | | 1.75 | | 2 | | 2.25 | |
| 0 | V | 0.32 | **0.30** | 0.33 | **0.32** | 0.33 | 0.33 | 0.34 | **0.30** |
| | Iter | 191 | **146** | 190 | **63** | 187 | **93** | 186 | **77** |
| | $M_{nd}$ | 0.0901 | 0.1088 | 0.0948 | 0.0976 | 0.0947 | 0.1044 | 0.0952 | 0.0925 |
| | $C_{index}$ | 0.8513 | 0.8192 | 0.8505 | 0.8330 | 0.8514 | 0.8364 | 0.8531 | 0.8364 |
| | $G_{index}$ | 0.1487 | 0.1808 | 0.1495 | 0.167 | 0.1486 | 0.1636 | 0.1469 | 0.1636 |
| | $\eta$ | / | 1.2 | / | 2.4 | / | 1.5 | / | 2.5 |
| 0.1 | V | 0.36 | **0.28** | 0.33 | **0.28** | 0.33 | **0.32** | 0.33 | **0.31** |
| | Iter | 165 | **97** | 215 | **124** | 216 | **81** | 214 | **179** |
| | $M_{nd}$ | 0.0986 | 0.0989 | 0.0959 | 0.1030 | 0.0960 | 0.0993 | 0.0955 | 0.1086 |
| | $C_{index}$ | 0.8428 | 0.8330 | 0.8464 | 0.8348 | 0.8489 | 0.8362 | 0.8495 | 0.8264 |
| | $G_{index}$ | 0.1572 | 0.1670 | 0.1536 | 0.1652 | 0.1511 | 0.1632 | 0.1505 | 0.1736 |
| | $\beta$ | / | 2.1 | / | 1.7 | / | 2 | / | 1.1 |
| 0.2 | V | 0.33 | **0.32** | 0.32 | **0.28** | 0.32 | 0.32 | 0.32 | 0.32 |
| | Iter | 230 | **105** | 230 | **128** | 228 | **63** | 228 | **62** |
| | $M_{nd}$ | 0.0922 | 0.1022 | 0.0942 | 0.0996 | 0.0940 | 0.0876 | 0.0943 | 0.1049 |
| | $C_{index}$ | 0.8578 | 0.8314 | 0.8500 | 0.8359 | 0.8489 | 0.8352 | 0.8516 | 0.8389 |
| | $G_{index}$ | 0.1422 | 0.1686 | 0.1500 | 0.1641 | 0.1511 | 0.1648 | 0.1484 | 0.1611 |
| | $\eta$ | / | 1.5 | / | 1.8 | / | 3.4 | / | 3.4 |
| 0.3 | V | 0.33 | **0.32** | 0.32 | **0.29** | 0.32 | **0.29** | 0.32 | **0.28** |
| | Iter | 244 | **73** | 264 | **220** | 216 | **173** | 258 | **163** |
| | $M_{nd}$ | 0.0924 | 0.0894 | 0.0942 | 0.0988 | 0.0944 | 0.1040 | 0.0941 | 0.0984 |
| | $C_{index}$ | 0.8553 | 0.8308 | 0.8492 | 0.8420 | 0.8506 | 0.8364 | 0.8495 | 0.8317 |
| | $G_{index}$ | 0.1447 | 0.1692 | 0.1508 | 0.1580 | 0.1494 | 0.1636 | 0.1505 | 0.1683 |
| | $\eta$ | / | 2.6 | / | 1.1 | / | 1.4 | / | 1.6 |
| 0.4 | V | 0.33 | **0.28** | 0.32 | **0.27** | 0.32 | **0.28** | 0.33 | **0.32** |
| | Iter | 284 | **253** | 310 | **192** | 304 | **249** | 286 | **120** |
| | $M_{nd}$ | 0.0932 | 0.1011 | 0.0947 | 0.0960 | 0.0948 | 0.1033 | 0.0946 | 0.0958 |
| | $C_{index}$ | 0.8527 | 0.8284 | 0.8477 | 0.8331 | 0.8497 | 0.8239 | 0.8530 | 0.8356 |
| | $G_{index}$ | 0.1473 | 0.1716 | 0.1523 | 0.1669 | 0.1503 | 0.1761 | 0.1470 | 0.1644 |
| | $\eta$ | / | 1 | / | 1.4 | / | 1.1 | / | 1.8 |
| 0.5 | V | 0.33 | **0.28** | 0.32 | **0.28** | 0.32 | **0.31** | 0.32 | **0.31** |
| | Iter | 337 | **160** | 368 | **186** | 360 | **97** | 358 | **100** |
| | $M_{nd}$ | 0.0931 | 0.0934 | 0.0942 | 0.0961 | 0.0946 | 0.0770 | 0.0940 | 0.0725 |
| | $C_{index}$ | 0.8523 | 0.8294 | 0.8489 | 0.8323 | 0.8513 | 0.8316 | 0.8497 | 0.8305 |
| | $G_{index}$ | 0.1477 | 0.1706 | 0.1511 | 0.1677 | 0.1487 | 0.1684 | 0.1503 | 0.1695 |
| | $\eta$ | / | 1.7 | / | 1.7 | / | 3 | / | 3.4 |

From the data in Table 5, it can be seen that for any different values of $\alpha$ and $\eta$, under the constraint of a maximum von Mises stress of 1.05, the adaptive AEPTO algorithm can effectively solve the minimum volume of cantilever beams in stress constrained optimization problems. AEPTO can achieve the minimum material volume fraction and therefore the minimum material mass, thus achieving the goal of lightweighting. Under the same parameters, when $q \in [1.5, 2.25]$ and $\alpha$ are set to 0, 0.1, 0.2, 0.3, 0.4, and 0.5, the best results obtained by the PTO algorithm are 0.32, 0.33, 0.32, 0.32, 0.32, and 0.32, respectively. The best results obtained by the AEPTO algorithm are 0.30, 0.28, 0.28, 0.27, and 0.28, which decrease by 6.3%, 15.2%, 12.5%, 12.5%, 15.6%, and 12.5%, respectively. It can be seen that for the topology structure of L-shaped beams, for different α, the performance improvement of AEPTO algorithm is relatively stable compared to the original PTO. The comparison indicators, grayscale indicators, and discrete indicators between AEPTO algorithm and the

original PTO algorithm are relatively stable with small differences. The results obtained from both algorithms are somewhat difficult in the manufacturing of beams. However, from the perspective of iteration times, it can be seen that AEPTO algorithm is significantly better than the PTO algorithm in terms of iteration times when solving the optimization problem shown in Figure 10. From the perspective of lightweighting, AEPTO algorithm can achieve better topological structures, higher utilization of material volume, material savings, and further reduce manufacturing costs.

According to the topology diagrams 13 (a) and 14 (e) of each algorithm, it can be observed that there are significant differences between the two optimal topology structures obtained by PTO algorithm and AEPTO algorithm. In addition, by observing the stress diagrams of the optimized structure, it can be seen that although the stress distribution of the optimized structure obtained by AEPTO algorithm is higher than that of the PTO algorithm, the stress distribution in these areas is still within the allowable stress range, indicating that the two optimized structures are safe and reliable. According to the stress diagram, the score results of the optimized structure show that the best optimized structure obtained by AEPTO algorithm is superior to that obtained by PTO algorithm in terms of strength to weight ratio.

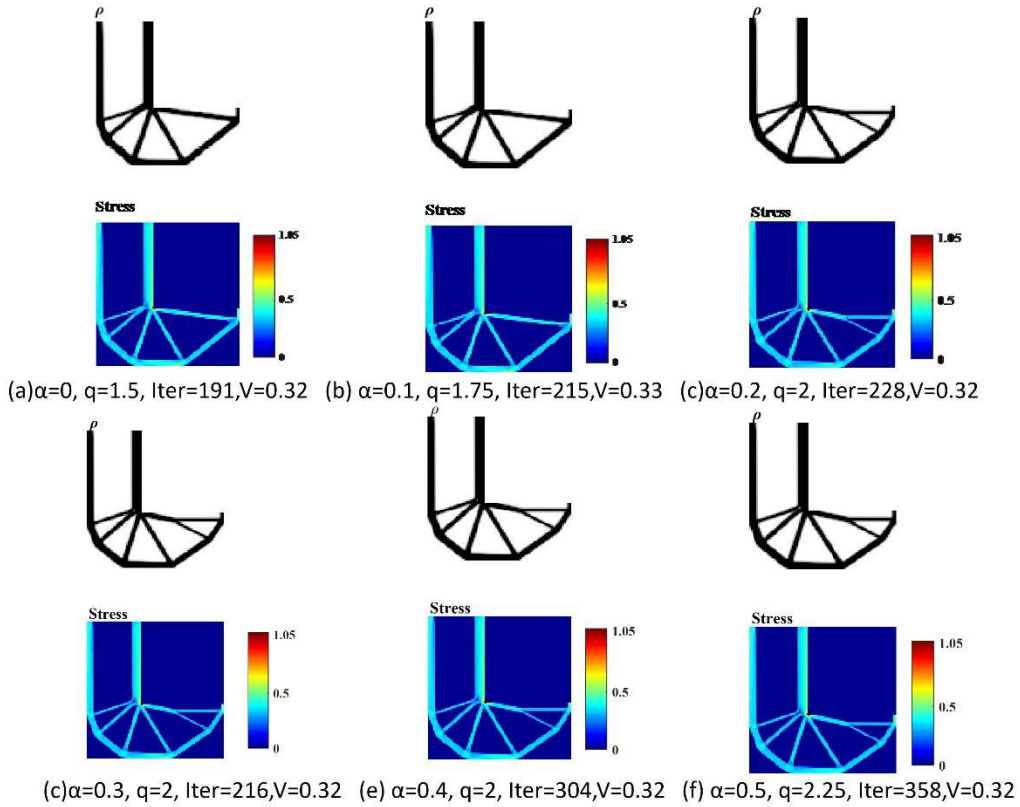



**Figure 13** Optimal Topological Structure of L-beam Obtained by PTO Algorithm.

Figure 15 shows the iteration history curves of the optimal objective function for each algorithm. Under the same constraints, AEPTO achieved essentially the same optimization results with fewer iterations compared to the original PTO algorithm. The law has improved the efficiency of the algorithm.

Based on the data from Figure 13 and Figure 14, as well as Table 5, overall, the AEPTO algorithm outperforms the original PTO algorithm in terms of lightweight and convergence when solving the topology problem of minimum volume cantilever beams under stress constraints. The introduction of Cauchy type filters, inverse tangent density update strategy, and dynamic historical balance coefficient has improved the ability of the new algorithm to obtain accurate solutions, improved the topology structure, and also increased the convergence speed of the new algorithm, which can save more materials and achieve the goal of lightweighting.

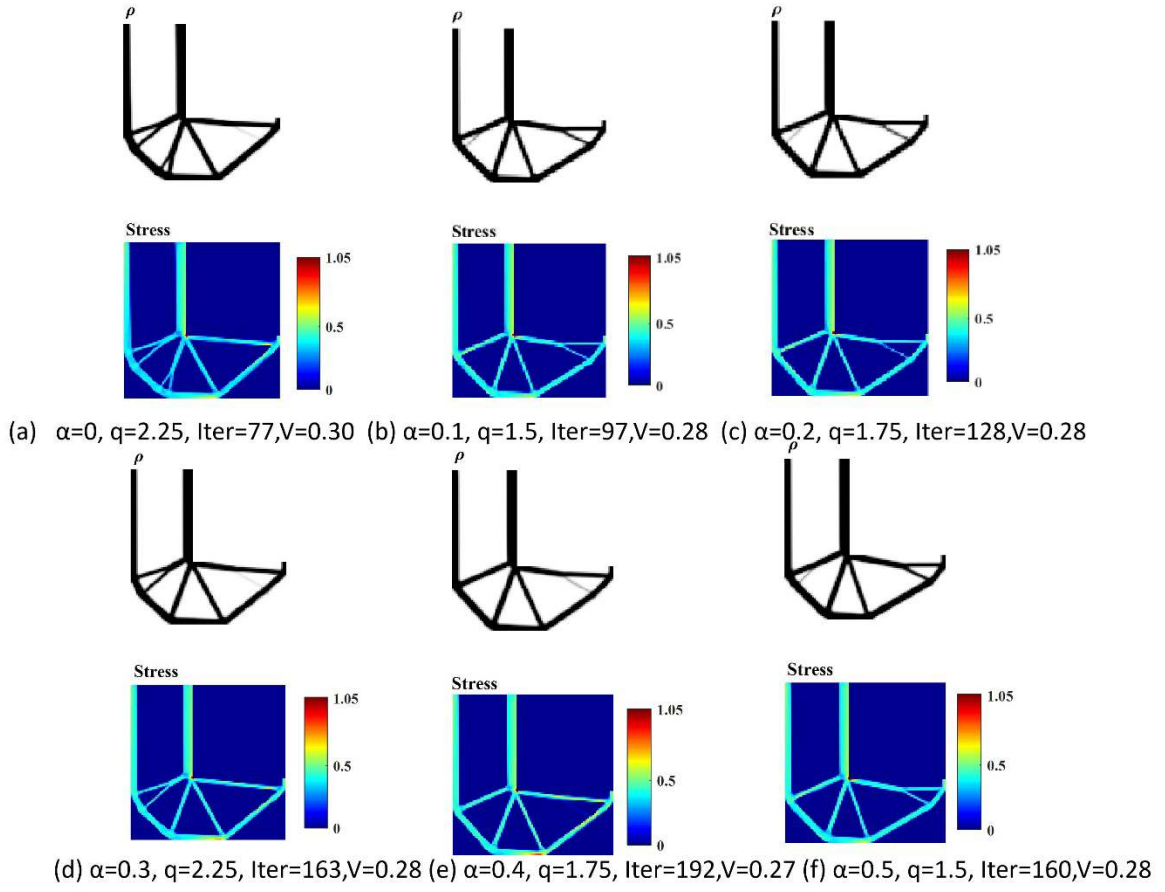



**Figure 14** Optimal Topological Structure of L-beam obtained by AEPTO algorithm.

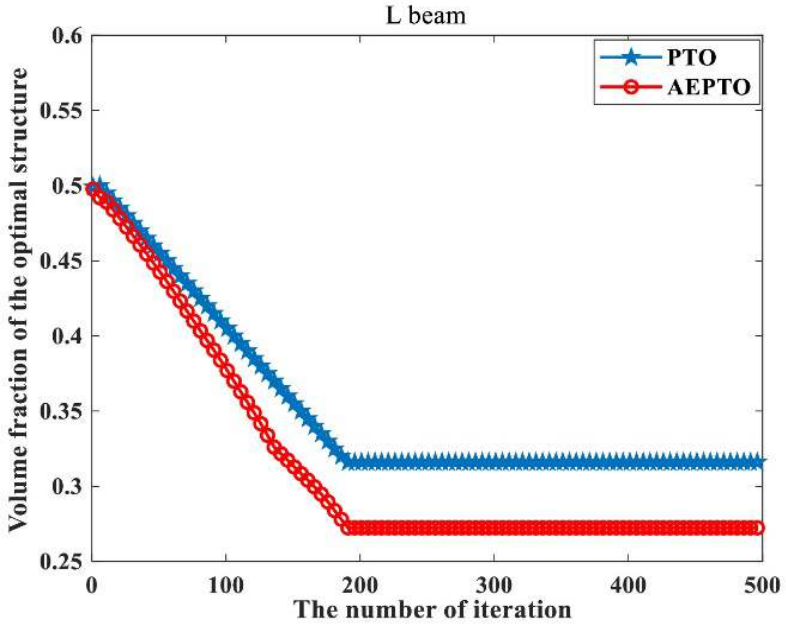



**Figure 15** Volume fraction convergence diagram of L beam optimal topology obtained by PTO and AEPTO algorithms.

### 5.5 MBB beam problem

Sigmund's MBB beam (2001) serves as the third example. Figure 16 shows the dimensions, boundaries, and externally applied loads of the design area. Considering the symmetry of the geometric structure, boundaries, and external load conditions of the MBB beam, we have considered the optimization problem of the half MBB beam shown in Figure 16. The

ratio of length, width, and thickness within the design area is 120:40:1. Due to symmetry, the beam is fixed at the left edge and simply supported at the lower right corner. An external downward normal load F=1 is applied to the upper left corner of the beam, which is subject to symmetry and vertical constraints, as shown in Figure 17. The material properties are listed in Table 1. The stress ratio influence coefficient is set to $q$=1, and the upper and lower boundaries of the density variable are [0,1]. The design domain is discretized into 120×40 (*nelx* ×*nely*) bilinear four node quadrilateral elements. Nodes and units are numbered uniformly in the order of top to bottom and left to right. In addition to the basic parameters, other parameters used by the algorithm also need to be separately set according to the requirements of the example and the research needs of the problem.

In the MBB beam, the control parameters for the optimization problem are set to $q$ ranging from 1.75 to 2.5 in increments of 0.25, $\alpha \in [0, 1]$, Here, due to excessive $\alpha$ leading to an increase in convergence times and excessive reliance on the optimal volume fraction accumulated by internal circulation, the value of α increases by 0.1 from 0 to 0.5. The final optimal topology index results of the L-beam obtained by setting the optimal control parameters for PTO and AEPTO algorithms are shown in Table 6. The meanings of the parameters and representation methods in the table are the same as those in Section 5.2. Figure 18 and 19 show the optimal topology results obtained by PTO algorithm and AEPTO algorithm with different $q$ under different $\alpha$, respectively. Figure 17 (a) to (f) correspond to the final optimal topology results of PTO when α takes the values of 0, 0.1, 0.2, 0.3, 0.4 and 0.5, respectively. Figure 18 (a) to (f) correspond to the final optimal topology results of AEPTO when $\alpha$ is set to 0, 0.1, 0.2, 0.3, 0.4, and 0.5, respectively.

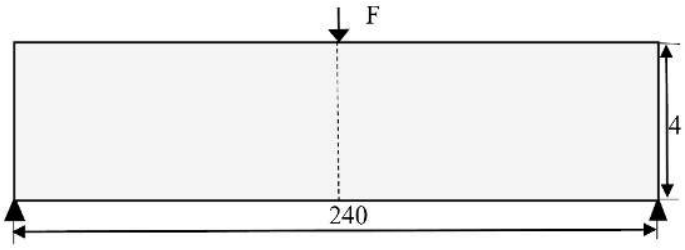



**Figure 16** Schematic Diagram of MBB Beam.

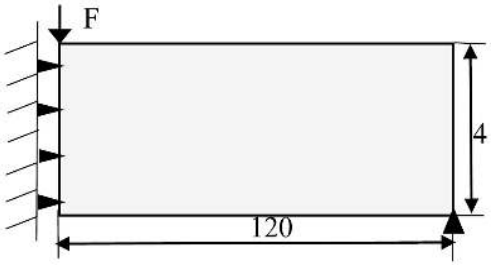



**Figure 17** Schematic diagram of right half of MBB beam.

From the data in Table 6 it can be seen that for any different values of α and η, under the constraint of a maximum von Mises stress of 1.05, the adaptive AEPTO algorithm can effectively solve the minimum volume of cantilever beams in stress constrained optimization problems. AEPTO can achieve the minimum material volume fraction and therefore the minimum material mass, thus achieving the goal of lightweighting. Under the same parameters, when $q \in [1.75, 2.5]$ and α are set to 0, 0.1, 0.2, 0.3, 0.4, and 0.5, the best results obtained by the PTO algorithm are 0.28, 0.25, 0.34, 0.36, 0.36, and 0.38, respectively. The best results obtained by the AEPTO algorithm are 0.25, 0.22, 0.23, 0.22, 0.21, and 0.21, reducing the performance by 10.7%, 12%, 32.4%, 38.9%, 41.7%, and 44.7%, respectively. It can be seen that for the topology structure of MBB beams, for different $\alpha$, the performance improvement of AEPTO algorithm is more significant compared to the original PTO algorithm. The differences in comparison metrics, grayscale metrics, and discrete metrics between the original PTO algorithm and AEPTO algorithm are relatively small, making them relatively stable. AEPTO algorithm outperforms the original PTO algorithm in at least 3 out of the 5 tested metrics. The results obtained from both algorithms are somewhat difficult in the manufacturing of beams. However, from the perspective of iteration times, it can be seen that AEPTO algorithm is significantly better than the PTO algorithm in terms of iteration times when solving the optimization problem shown in Figure 17. From a lightweight perspective, AEPTO algorithm can achieve better topological structures, higher utilization of material volume, material savings, and further reduce costs.

**Table 6** Optimization results of MBB beam obtained by PTO and AEPTO algorithm considering control parameter setting.

| Evaluation metric | | Algorithms | | | | | | | |
|---|---|---|---|---|---|---|---|---|---|
| | | PTO | AEPTO | PTO | AEPTO | APTO | EAPTO | PTO | AEPTO |
| **α** | ***q*** | **1.75** | | **2** | | **2.25** | | **2.5** | |
| 0 | V | 0.32 | **0.25** | 0.31 | **0.28** | 0.35 | **0.30** | 0.28 | **0.28** |
| | Iter | 197 | **144** | 206 | **209** | 170 | **206** | 243 | **164** |
| | $M_{nd}$ | 0.1119 | 0.0966 | 0.1030 | 0.0915 | 0.1099 | 0.0982 | 0.0837 | **0.0935** |
| | $C_{index}$ | 0.8123 | 0.8356 | 0.8321 | 0.8542 | 0.8202 | 0.8442 | 0.8725 | **0.8450** |
| | $G_{index}$ | 0.1877 | **0.1644** | 0.1679 | **0.1458** | 0.1798 | **0.1558** | 0.1275 | 0.1550 |
| | $\eta$ | / | 1.5 | / | 1.5 | / | 1.5 | / | 1 |
| 0.1 | V | 0.36 | **0.23** | 0.30 | **0.22** | 0.34 | **0.25** | 0.25 | 0.25 |
| | Iter | 179 | **143** | 248 | **94** | 205 | **91** | 325 | **109** |
| | $M_d$ | 0.0931 | **0.0960** | 0.1048 | 0.0868 | 0.1094 | 0.0859 | 0.0836 | **0.0872** |
| | $C_{index}$ | 0.8475 | **0.8402** | 0.8317 | 0.8471 | 0.8173 | 0.8435 | 0.8692 | **0.8575** |
| | $G_{index}$ | 0.1525 | 0.1598 | 0.1683 | **0.1529** | 0.1827 | **0.1565** | 0.1308 | 0.1425 |
| | $\eta$ | / | 1.5 | / | 2.9 | / | 2.9 | / | 2.7 |
| 0.2 | V | 0.36 | **0.25** | 0.36 | **0.24** | 0.36 | **0.25** | 0.34 | **0.23** |
| | Iter | 209 | **127** | 200 | **138** | 209 | **177** | 237 | **127** |
| | $M_d$ | 0.0963 | **0.1089** | 0.0959 | 0.0924 | 0.0964 | 0.0925 | 0.1004 | 0.0883 |
| | $C_{index}$ | 0.8498 | **0.8135** | 0.8362 | 0.8398 | 0.8419 | **0.8410** | 0.8298 | 0.8548 |
| | $G_{index}$ | 0.1502 | 0.1865 | 0.1638 | **0.1602** | 0.1581 | 0.1590 | 0.1702 | **0.1452** |
| | $\eta$ | / | 1.7 | / | 1.8 | / | 1.5 | / | 2.5 |
| 0.3 | V | 0.36 | **0.22** | 0.39 | **0.38** | 0.36 | **0.24** | 0.37 | **0.25** |
| | Iter | 216 | **109** | 180 | **130** | 224 | **111** | 211 | **114** |
| | $M_d$ | 0.0976 | 0.0864 | 0.0939 | **0.0998** | 0.0971 | 0.0792 | 0.0953 | 0.0821 |
| | $C_{index}$ | 0.8427 | **0.8277** | 0.8535 | **0.8479** | 0.8365 | 0.8519 | 0.8496 | **0.8446** |
| | $G_{index}$ | 0.1573 | 0.1723 | 0.1465 | 0.1521 | 0.1635 | **0.1481** | 0.1504 | 0.1594 |
| | $\eta$ | / | 2.9 | / | 1 | / | 3.5 | / | 2.5 |
| 0.4 | V | 0.38 | **0.22** | 0.36 | 0.38 | **0.37** | **0.21** | 0.39 | **0.22** |
| | Iter | 209 | **124** | 251 | 208 | 246 | **141** | 228 | **175** |
| | $M_d$ | 0.0943 | 0.0838 | 0.0967 | **0.1081** | 0.0984 | 0.0855 | 0.0972 | 0.0890 |
| | $C_{index}$ | 0.8483 | **0.8265** | 0.8446 | **0.8381** | 0.8425 | 0.8458 | 0.8427 | 0.8500 |
| | $G_{index}$ | 0.1517 | 0.1735 | 0.1554 | 0.1619 | 0.1575 | **0.1542** | 0.1573 | **0.1500** |
| | $\beta$ | / | 3 | / | 0.5 | | 2.5 | / | 2 |
| 0.5 | V | 0.38 | 0.38 | 0.39 | **0.24** | 0.38 | **0.21** | 0.38 | **0.22** |
| | Iter | 252 | **244** | 246 | **157** | 255 | **150** | 261 | **202** |
| | $M_d$ | 0.0953 | **0.1038** | 0.0966 | **0.0969** | 0.0974 | 0.0893 | 0.0981 | 0.0865 |
| | $C_{index}$ | 0.8452 | **0.8435** | 0.8467 | **0.8165** | 0.8438 | **0.8252** | 0.8446 | 0.8508 |
| | $G_{index}$ | 0.1548 | 0.1565 | 0.1533 | 0.1835 | 0.1563 | 0.1748 | 0.1569 | **0.1492** |
| | $\eta$ | / | 0.5 | / | 2 | / | 3 | / | 2 |

According to the lightest topology structure diagrams 18 (b) and 19 (f) of the two algorithms, it can be observed that there are significant differences between the two optimal topology structures obtained by PTO algorithm and AEPTO algorithm. Furthermore, by observing the stress diagrams of the optimized structures shown in Figures 18 and 19, although the stress distribution of the optimized structure obtained by the AEPTO algorithm is higher than that of the PTO algorithm, the stress distribution in these areas is still within the allowable stress range, indicating that both optimized structures are safe and reliable. According to the stress diagram, the score results of the optimized structure show that the best optimized structure obtained by AEPTO algorithm is superior to that obtained by PTO algorithm in terms of strength to weight ratio.

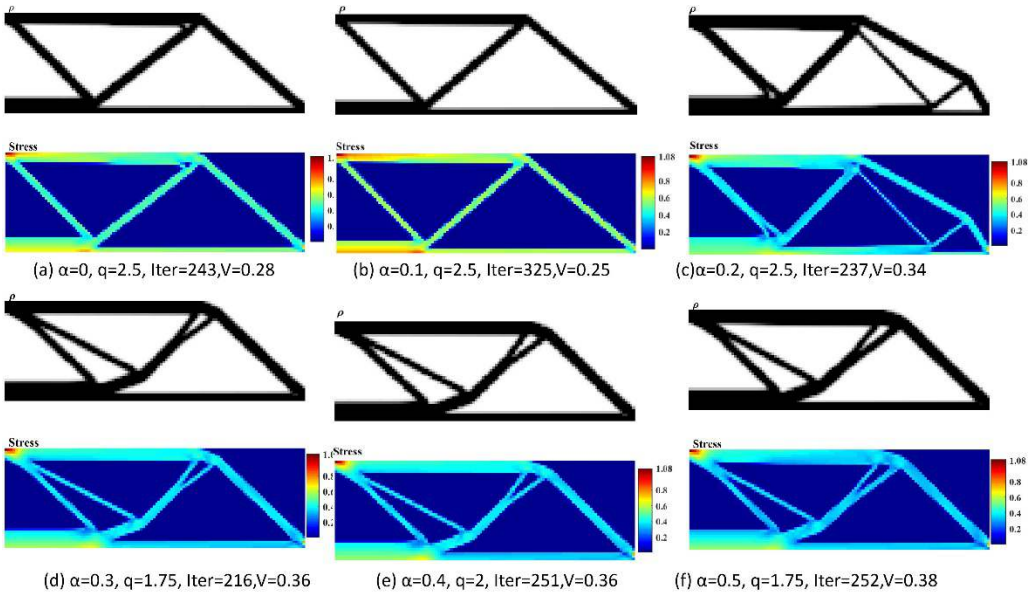



**Figure 18** Optimal Topological Structure of MBB beam obtained by PTO Algorithm.

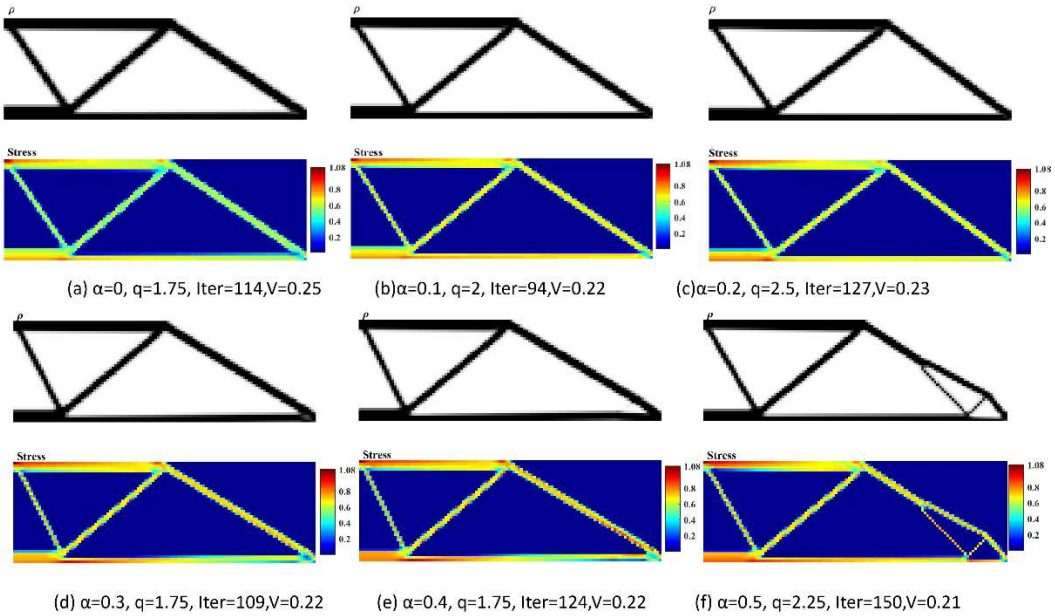



**Figure 19** Optimal Topological Structure of MBB beam Obtained by AEPTO Algorithm.

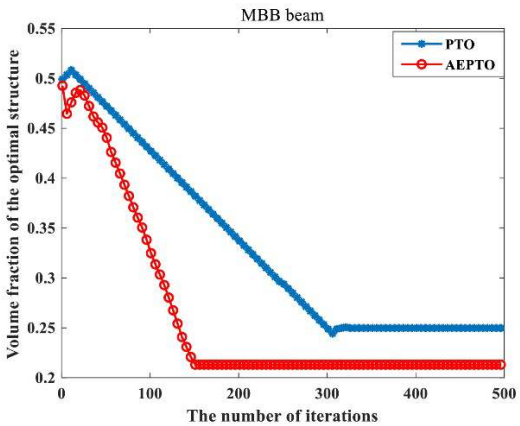



**Figure 20** Volume fraction convergence diagram of MBB beam optimal topology obtained by PTO and AEPTO algorithms.

Figure 20 shows the iteration history curves of the optimal objective function for each algorithm. Under the same constraints, AEPTO achieved essentially the same optimization results with fewer iterations, improving the efficiency of the algorithm compared to the original PTO algorithm.

Based on the data from Figures 18 and 19, as well as Table 6, overall, AEPTO algorithm outperforms the original PTO algorithm in terms of lightweight and convergence when solving the topology problem of minimum volume cantilever beams under stress constraints. The introduction of Cauchy type filters, inverse tangent density update strategy, and dynamic historical balance coefficient has improved the ability of the new algorithm to obtain accurate solutions, improved the topology structure, and also increased the convergence speed of the new algorithm, which can save more materials and achieve the goal of lightweighting.

## 6 Conclusions

To overcome the limitations of the PTO algorithm, this study focuses on the minimum volume fraction problem and modifies the interpolation model, filter, density variable update scheme, and the update method of density variables in the inner loop and main loop, while introducing a dynamically adaptive balance coefficient. The effectiveness and practicality of the improved scheme are verified through three numerical examples.

Based on the data presented in Figures 10, 11, 14, 15, 19, 20 and Tables 3-6, in general, when solving the topology optimization problems of cantilever beams, L-shaped beams, and MBB beams with the objective of minimum volume under stress constraints, the AEPTO algorithm is significantly superior to the original PTO algorithm in terms of lightweight performance and convergence. The introduction of the Cauchy-type filter and the arctangent-based density update strategy enhances the new algorithm's ability to obtain accurate solutions, improves the topological structure, contributes to accelerating the convergence speed of the new algorithm, and strengthens its capability to achieve the minimum optimal material volume fraction. This implies that more materials can be saved while meeting the stress constraints. The use of the improved density filter and the new density variable update scheme in the inner loop can optimize the topological structure of the new algorithm and enhance its ability to obtain accurate solutions. The application of the new target material volume update scheme can improve the robustness and convergence of the new algorithm. Additionally, the introduction of the adaptive balance coefficient into the AEPTO algorithm helps increase the number of iterations of the AEPTO algorithm while improving its convergence performance. This further demonstrates the practicality and applicability of the proposed method, providing an idea and solution approach for structural lightweight problems and topology optimization structures.

To further demonstrate the superiority and reliability of the proposed method, future work will construct a unified simulation platform. Under the same load, mesh, and constraint conditions, the performance differences between AEPTO, OC, and MMA will be systematically compared from three dimensions: topological rationality, computational efficiency, and engineering manufacturability.

## Acknowledgments

This work is supported by the Scientific Research Program Funded by Shaanxi Provincial Education Department (Program No.25JK0451).

**Data Availability:** All numerical examples and results presented in this paper are fully reproducible using the adaptive enhanced proportional topology optimization algorithm described in the manuscript, along with the open-source software MATLAB/ANSYS. Detailed parameter settings, including filter radius, penalty factors, mesh size, and boundary conditions, are provided in the manuscript. No external datasets were used in this study.

**Editor:** Marcilio Alves.

## References

Amaral, R.R., Borges, J.A., & Gomes, H.M. (2022). Proportional topology optimization under reliability-based constraints. Journal of Applied and Computational Mechanics, 8, 319-330. https://doi.org/10.22055/JACM.2021.38440.3226.

Andreassen, E., Clausen, A., Schevenels, M., Lazarov BS, & Sigmund, O. (2011). Efficient topology optimization in MATLAB using 88 lines of code. Structural and Multidisciplinary Optimization, 43(1), 1-16. https://doi.org/10.1007/s00158-010-0594-7.

Bendsoe, M.P., Kikuchi, N. (1988). Generating optimal topologies in structural design using a homogenization method. Computer Methods in Applied Mechanics and Engineering,71(2), 97-224. https://doi.org/10.1016/0045-7825(88)90086-2.

Biyikli, E., To, A.C. (2015). Proportional topology optimization: a new nonsensitivity method for solving stress constrained and minimum compliance problems and its implementation in MATLAB. Plos One, 10(12), 1-23. https://doi.org/10.1371/journal.pone.0145041.

Bruns, T.E., Tortorelli, D.A .(2001). Topology optimization of non-linear elastic structures and compliant mechanisms. Computer Methods in Applied Mechanics and Engineering, 190(26), 3443-3459. https://doi.org/10.1016/S0045-7825(00)00278-4.

Cheng, W., Wang, H., Zhang, M., & Du, R. (2021). Improved proportional topology optimization algorithm for minimum volume problem with stress constraints. Engineering Computations, 38(1), 392-412. https://doi.org/10.1108/EC-12-2019-0560.

Dantzig, G.B.(1963). Linear programming and its extensions, Princeton University Press, Princeton, NJ.

Fleury, C., Braibant, V. (1986). Structural optimization: a new dual method using mixed variables. International Journal for Numerical Methods in Engineering, 23(3), 409-428. https://doi.org/10.1002/nme.1620230307.

Garcia-Lopez, N.P., Sanchez-Silva, M., Medaglia, A.L., Chateauneuf, A. (2011). A hybrid topology optimization methodology combining simulated annealing and SIMP. Computers & Structures, 89(15),1512-1522. https://doi.org/10.1016/j.compstruc.2011.04.008.

Guo, G.K. (2025). Topology optimization of compliant mechanisms under displacement feedback control with time delay. Mechanism and Machine Theory, 211, 106041. https://doi.org/10.1016/j.mechmachtheory.2025.106041.

Holmberg, E., Torstenfelt, B., Klarbring, A. (2013). Stress constrained topology optimization.Structural and Multidisciplinary Optimization, 48(1): 33-47. https://doi.org/10.1007/s00158-012-0880-7.

Hussain, A., Cheng, W.M., Du, R. (2025). Advancements in Lightweight Structure Design: Proportional Topology Optimization and Isogeometric Analysis. International Journal of Computational Methods, 22(10), 2025. https://doi.org/10.1142/S021987622550019.

Jang, I.G., Kim, K., Kwak, B.M. (2014). Conceptual and basic designs of the mobile harbor crane based on topology and shape optimization. Structural and Multidisciplinary Optimization, 50 (3), 505-515. https://doi.org/10.1007/s00158-014-1073-3.

Kongwat, S., Hasegawa, H. (2019). Optimization on mechanical structure for material nonlinearity based on proportional topology method. Journal of Advanced Simulation in Science and Engineering, 6(2), 354-366. https://doi.org/10.15748/jasse.6.354.

Lee, K., Ahn, K., Yoo, J. (2016). A novel P-norm correction method for lightweight topology optimization under maximum stress constraints. Computers & Structures, 171, 18-30. https://doi.org/10.1016/j.compstruc.2016.04.005.

Lee, K.S., Geem, Z.W. (2004). A new structural optimization method based on the harmony search algorithm. Computers & Structures, 82(9) :781-798. https://doi.org/10.1016/j.compstruc.2004.01.002.

Li, C., Kim, I.Y., Jeswiet, J. (2015). Conceptual and detailed design of an automotive engine cradle by using topology, shape, and size optimization. Structural and Multidisciplinary Optimization, 51(2), 547-564. https://doi.org/10.1007/s00158-014-1151-6.

Li, L., Khandelwal, K. (2015). Volume preserving projection filters and continuation methods in topology optimization. Engineering Structures, 85, 144-161. https://doi.org/10.1016/j.engstruct.2014.10.052.

Li, W., Cui, M., Wang, X., Gao, M. (2024). An enhanced proportional topology optimization method with new density filtering weight function for the minimum compliance problem. Mechanics Based Design of Structures and Machines, 53(4), 2666-2695. https://doi.org/10.1080/15397734.2024.2412753.

Luo, Y.J., Wang, M.Y., Kang, Z. (2013). An enhanced aggregation method for topology optimization with local stress constraints. Computer Methods in Applied Mechanics and Engineering, 254, 31-41. https://doi.org/10.1016/j.cma.2012.10.019.

Madeira, JFA., Rodrigues, H., Pina, H. (2005). Multi-objective optimization of structures topology by genetic algorithms. 36(1), 21-28. https://doi.org/10.1016/j.advengsoft.2003.07.001.

Nguyen, M.N., Tran, MT., Nguyen, H.Q., Bui, T.Q .(2023). A multi-material Proportional Topology Optimization approach for compliant mechanism problems.European Journal of Mechanics-A/ Solids, 100, 104957. https://doi.org/10.1016/j.euromechsol.2023.104957.

París, J., Navarrina, F., Colominas, I., Casteleiro, M. (2009). Topology optimization of continuum structures with local and global stress constraints. Structural and Multidisciplinary Optimization, 39 (4), 419-437. https://doi.org/10.1007/s00158-008-0336-2.

Sigmund, O. (2001). A 99 line topology optimization code written in Matlab. Structural and Multidisciplinary Optimization, 21(2), 120-127. https://doi.org/10.1007/s001580050176.

Sigmund, O., Maute, K. (2013) .Topology optimization approaches. Structural and Multidisciplinary Optimization, 48 (6), 1031-1055. https://doi.org/10.1007/s00158-013-0978-6.

Sigmund, O, (2007). Morphology-based black and white filters for topology optimization. Structural and Multidisciplinary Optimization, 33(4-5), 401-424. https://doi.org/10.1007/s00158-006-0087-x.

Svanberg, K .(1987). The method of moving asymptotes-a new method for structural optimization. International Journal for Numerical Methods in Engineering, 24(2), 359-373. https://doi.org/10.1002/nme.1620240207.

Van Dijk, N.P., Maute, K., Langelaar, M., Van Keulen, F. (2013). Level-set methods for structural topology optimization: a review. Structural and Multidisciplinary Optimization, 48(3), 437-472. https://doi.org/10.1007/s00158-013-0912-y.

Vemaganti, K., Lawrence, W.E. (2005). Parallel methods for optimality criteria-based topology optimization. Computer Methods in Applied Mechanics and engineering, 194(34), 3637-3667. https://doi.org/10.1016/j.cma.2004.08.008.

Wang, F.W., Lazarov, B.S., Sigmund, O. (2011). On projection methods, convergence and robust formulations in topology optimization. Structural and Multidisciplinary Optimization, 43 (6): 767-784. https://doi.org/10.1007/s00158-010-0602-y.

Xu, S.L., Cai, Y.W., Cheng, G.D. (2010). Volume preserving nonlinear density filter based on heaviside functions. Structural and Multidisciplinary Optimization, 41(4), 495-505. https://doi.org/10.1007/s00158-009-0452-7.

Yang, D.X., Liu, H. L., Zhang, W. S., Li, S. (2018). Stress-constrained topology optimization based on maximum stress measures. Computers and Structures, 198: 23-39. https://doi.org/10.1016/j.compstruc.2018.01.008.

Yoo, K.S., Han, S.Y. (2015). Topology optimum design of compliant mechanisms using modified ant colony optimization. Journal of Mechanical Science and Technology, 29(8), 3321-3327. https://doi.org/10.1007/s12206-015-0729-2.

Zhang, Y. F. (2018). Structural topology optimization based on proportional topology optimization method, Thesis, Mechanical Engineering. Xidian University, Shaanxi, China, 2018.